1-1-1998

3D characterization of Magnetic Flux Leakage signals : a data fusion approach

Vaishali Vilas Kamat
Iowa State University

3D characterization of Magnetic Flux Leakage signals: A data fusion approach

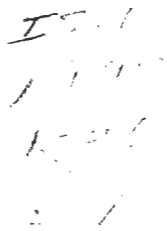

by

Vaishali Vilas Kamat

A thesis submitted to the graduate faculty

in partial fulfillment of the requirements for the degree of

MASTER OF SCIENCE

Major: Electrical Engineering

Major Professor: Dr. Satish Udpa

Iowa State University

Ames, Iowa

1998

Graduate College
Iowa State University

This is to certify that the Master's thesis of

Vaishali Vilas Kamat

has met the thesis requirements of Iowa State University

Signatures have been redacted for privacy

TABLE OF CONTENTS

ACKNOWLEDGEMENTS

The very first and the biggest vote of thanks goes to my advisor Dr. Satish Udpa. With his immense knowledge of the subject and his excellent abilities as a teacher, he has been a constant source of guidance and motivation. His understanding and patient nature always made it simple to approach him with the smallest to the toughest of problems.

I appreciate the guidance and help from Dr. William Lord and Dr. Lalita Udpa, and thank them for agreeing to serve on my committee.

I also thank Dr. Jennifer Davidson and Dr. Edward Jaselskis who took the time to serve on my committee.

I am grateful to Dr. Shreekanth Mandayam who, during my first year here, extended his help and assistance, when as a new graduate student, I needed it the most.

I have words of gratitude for the members of the Materials Characterization Research Group who have made these two years of my graduate program, a very pleasant and enjoyable working experience.

Last but not the least, I would like to thank my dear parents, who not only gave me this chance to pursue graduate studies, but were also there for me at every step of the way, like two solid pillars of support !

1. INTRODUCTION

1.1 Nondestructive Evaluation (NDE)

" Non-destructive testing has clearly no defined boundaries" - R. Halmshaw

Ever since society first realized the fallibility of people and their machines, it has recognized the need to inspect these machines in order to prevent their failures. To improve their quality and to ensure safety, all components and structures need to be inspected regularly, for defects or faults which may adversely affect their overall structural integrity. A variety of testing schemes have evolved, some destructive and some non destructive. The practical benefits of nondestructive testing are obvious, provided the results are reliable.

Nondestructive testing techniques are those which leave the components undamaged after inspection and can be characterized in general as, active or passive and surface, near-surface or volumetric [1]. Active techniques are those in which energy in some form is introduced into or onto the specimen. The material/ energy interaction process is observed to detect and possibly characterize the presence of an anomaly. Magnetostatic, eddy current, ultrasonic, and radiographic NDE methods fall into this category. Passive techniques monitor or observe the item in question in the "as-is" state under the influence of a typical load environment. The presence of a defect is then determined by some response or reaction from the specimen. Acoustic emission, vibration analysis and residual magnetic techniques are examples of passive techniques. The word "defect" in NDE is applied only to a condition which will interfere with the safe or satisfactory operation of the part in question. The inverse

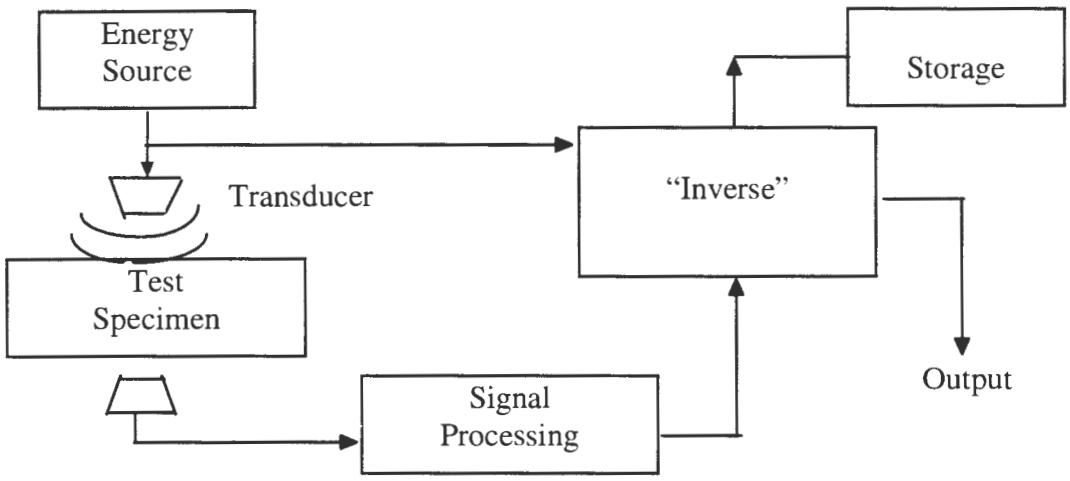

Figure 1.1. Typical NDE system [2].

problem attempts to determine the state of the test specimen by estimating the size, shape and location of the defect. A typical NDE system is shown in Figure 1.1 [2].

Choosing the right NDE technique for a particular application is as important as the evaluation itself. Factors which might affect this choice include size, orientation, and location of the flaw, type of material, etc. Detection of small flaws requires more sophisticated techniques than detection of larger flaws. Magnetic techniques can be applied only to ferromagnetic materials while eddy current techniques can be applied only to conducting materials. In many situations, prior defect history of the test specimen may provide additional information needed to choose the most appropriate testing technique.

1.2 Data Fusion In NDE

Data fusion deals with the synergistic combination of information made available by various sources/ sensors, in order to provide a better understanding of the scene [3]. The fused data not only reflects the information collected by every source, but also provides an

insight into information that cannot be inferred by looking at data from each source individually. There is considerable freedom with regard to the choice of sensors used for fusion; hence there is a certain ambiguity associated with the term data fusion. This work confines itself to approaches using multiple sensors and methods to combine data collected by them.

Data fusion offers several advantages over the use of a single sensor. Redundant information can be obtained by using many sensors; this reduces the uncertainty associated with the measurements and increases their reliability and accuracy. Complementary information can be obtained with the help of the many sensors as each sensor may perceive the features differently. Fusion also increases the speed with which information is obtained as many sensors together can used to build parallelism in the operation. Fusion may also be cost effective in cases where it might be cheaper and easier to integrate several simple sensors to collect information rather than building one complicated and expensive sensor capable of collecting the equivalent information. The role of multisensor integration in the overall operation of a system can be defined as the degree to which each of the above four aspects are present in the information presented by the sensors to the system.

Data fusion has been used in the present work, to fuse signals from two sensors providing complementary information. The concept in general and the fusion scheme used in the present work are explained in details in chapter 4.

1.3 Overview Of Thesis

NDE is of special importance in the inspection of large and expensive structures like nuclear reactors, aircraft, pipelines, etc. The accurate detection and characterization of flaws

can not only save human life and property, but also cut down manufacturing and inspection costs. This thesis deals with nondestructive evaluation of natural gas transmission pipelines using Magnetic Flux Leakage (MFL) techniques. An effort has been made to solve the inverse problem by characterizing the MFL signals using artificial neural networks.

Chapter 2 describes in detail, the MFL technique for NDE and also gives a brief introduction to the task of inspecting gas transmission pipelines.

Chapter 3 presents artificial neural networks as tools for signal characterization. An introduction to neural networks is provided and the Radial Basis Function (RBF) network is described in greater detail.

Chapter 4 provides review of data fusion and the various techniques that can be used for fusion. The particular scheme used in this work is also explained. Further, the chapter provides details regarding signal processing and feature extraction techniques used for data analysis and the algorithms used for determining the cluster centers for the RBF network.

Chapter 5 describes the actual inspection process and the experimental setup used for data collection. It presents the results obtained using this approach and conclusions that may be drawn on the basis of results obtained to date. The thesis concludes with a discussion on areas that may be explored in the future.

2. MAGNETIC FLUX LEAKAGE (MFL) TECHNIQUES

2.1 MFL Concepts

The Magnetic Flux Leakage method of flaw detection is based on the fact that a near-surface discontinuity in the geometry or magnetic properties of a magnetized body causes a localized perturbation in the field just outside the body. Thus an anomaly or crack can be detected by searching the surface of a specimen for localized fluctuations in the magnetic field [4]. The MFL technique represents a variation of the Magnetic Particle Inspection (MPI) method. It however, overcomes the drawback of the latter in that, it can also be used for inspection of areas that are not visually accessible (e.g.: the inside of pipelines). Another advantage associated with the MFL technique is the fact that the information generated by the inspection process can be readily analyzed using modern computer based techniques.

A magnetic field is responsible for the force of attraction between a piece of steel and a magnet. The strength and direction of this field is typically shown using "flux lines". To understand the origin of leakage fields [5], consider an unmagnetized billet with a surface flaw, as shown in Figure 2.1. Let the cross-sectional area of the billet and that of the flaw be 'A' and 'a' units, respectively. Therefore, the cross-sectional area of the "sound" portion of the billet in the vicinity of the flaw is (A-a) units. Consider a situation where the billet is placed in a uniform magnetizing field **H**; let the field induced in the sound portion of the billet be B_1 (webers/m^2).

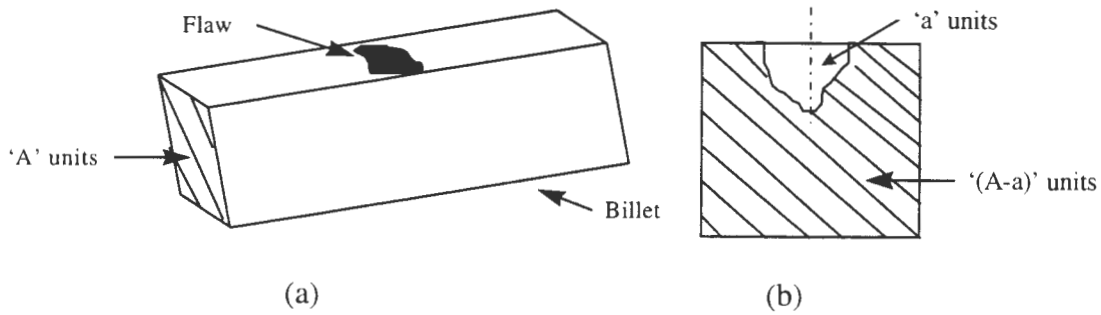

Figure 2.1 (a)Billet with defect (b) Cross-section through flaw [5].

This corresponds to a point P to the right of μ_{max} on the permeability curve, as seen in Figure 2.2. The corresponding point on the normal induction curve is Q and the total flux passing through the sound portion of the billet is B_1A (webers). Assuming that the same amount of flux has to pass through the reduced billet area in the vicinity of the flaw, the flux density in this section increases from B_1 to $B_2 = B_1A/(A-a)$ (webers/m^2).

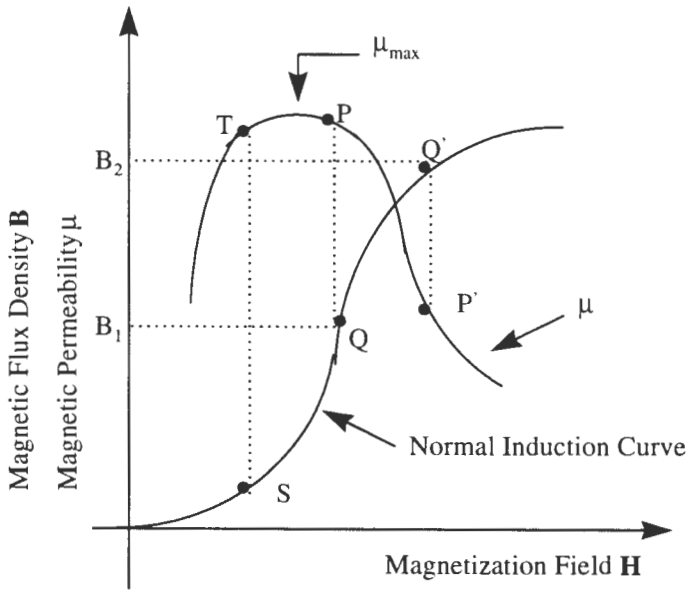

Figure 2.2. Magnetic characteristics of the billet material [5].

This local increase in the flux density moves the operating point on the induction curve from Q to Q' and therefore results in a decrease in the local permeability from P to P'. This contributes to a set of conflicting demands in the vicinity of the flaw. The flux density must increase due to the reduced cross-sectional area, but this drives the local permeability to a value lower than that of the surroundings. Consequently, some flux "leaks" into the surrounding medium and is termed as the leakage field, as shown in Figure 2.3.

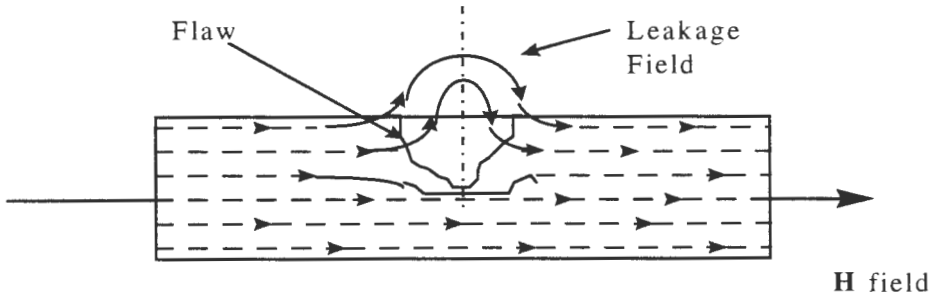

Figure 2.3. Leakage field due to a surface flaw [5].

The measurement of the leakage field allows the detection of surface and/ or near-surface flaws in materials and forms the basis of magnetic NDE techniques. A full measurement of the leakage field can be obtained by measuring its components along the tangential (axial), normal (radial) and circumferential directions. In practice, the measurement is often confined to the axial component only despite the fact that the other two components carry additional information relating to the flaw. Figure 2.4 shows the axial, radial and circumferential components of the leakage field signal produced by a typical mechanical damage defect.

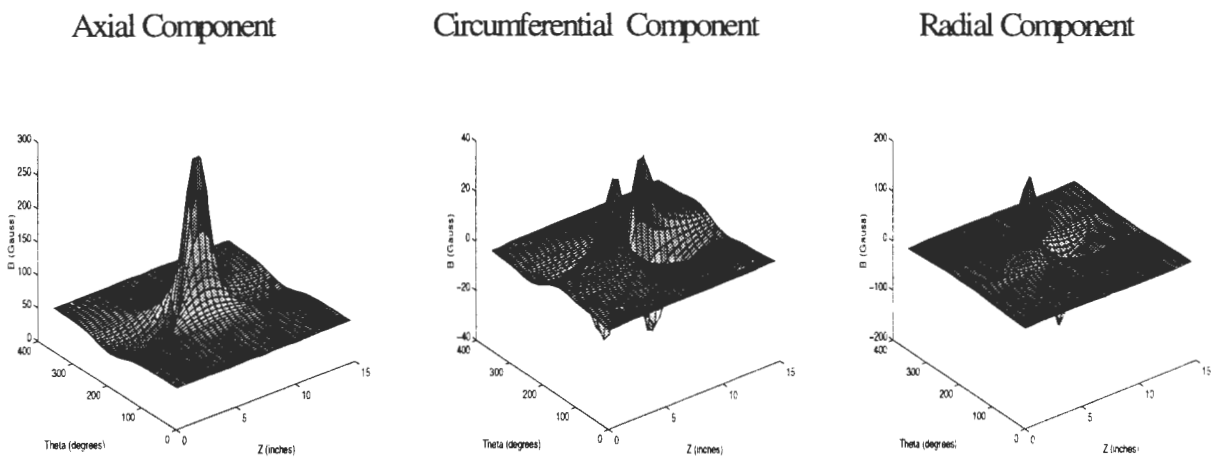

Figure 2.4. Leakage field components.

If, however, the flaw is located much below the surface of the specimen, the surrounding material tends to smooth out the distortion of the field due to this sub-surface flaw and a very small perturbation in the field results at the surface. It is therefore difficult to detect deep sub-surface flaws using this method.

Sensors used to detect and record perturbations can be of several types but the most commonly used ones are induction coils and Hall effect probes. A schematic view of the latter, which has been used in this study, is shown in Figure 2.5. The Hall probe uses a Hall effect element to convert field intensity to a voltage. The charge carriers in a current carrying conductor are deflected by a magnetic field, as a result of which the Hall probe produces a voltage across the sensor element that is proportional to the product of current I and the magnetic field intensity H.

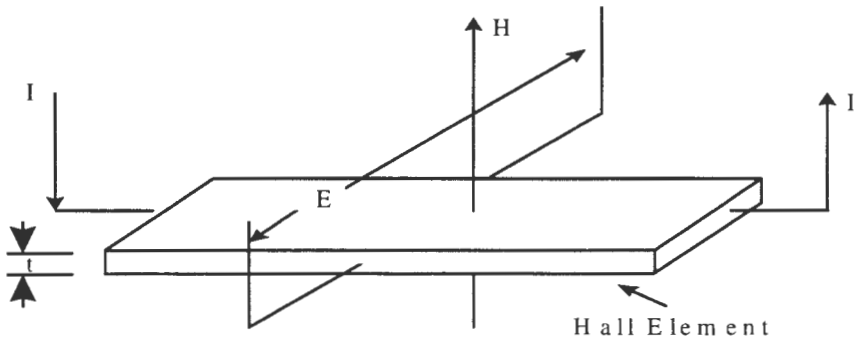

$E = (R/t)\ I \times H$ where,

E = Potential in Volts
R = Hall coefficient in Volt-cm / Ampere-Gauss
I = Current in Amperes
H = Magnetic field strength in Gauss
t = Thickness of Hall element in centimeters

Figure 2.5. Schematic diagram of the Hall effect probe [4].

The Hall effect occurs for all conducting materials. Semiconductors doped with impurities are commonly used as Hall elements. Maximum sensitivity is achieved when the Hall coefficient (R) is large and the thickness of the element (t) is small. A typical Hall element used for measurement of leakage fields would be 1 mm long, 0.5 mm wide and 0.05 mm thick.

The SI units for field intensity H and flux density B are Henrys (Ampere/meter) and Tesla (Weber/meter^2). However, most instruments in use in the U.S. are calibrated in Oersteds and Gauss respectively. The relation between the two systems of measurement are :

$$1\ \text{Oe} = 79.58\ \text{A/m} \quad \text{and} \quad 1\ \text{gauss} = 10^{-4}\ \text{Wb/m}^2$$

NDE systems using MFL techniques have been used for inspection of rotationally symmetric cylindrical parts like tubes, pipes, bars, rods, etc. Special purpose systems have

also been devised to inspect parts like helicopter rotor blades, gear teeth, artillery projectiles, etc.

This thesis focuses its attention on systems using MFL techniques for inspection of natural gas transmission pipelines.

2.2 Inspection Of Gas Pipelines

The natural gas industry is a significant commercial entity in the US. Over 30% of the energy produced domestically is derived from natural gas [6]. Gas produced at wells is typically transported through a vast pipeline network consisting of 280,000 miles of gas transmission lines, 90,000 miles of gathering lines and 835,000 miles of distribution lines to customer locations. It is therefore of utmost importance to ensure the safety and integrity of the pipes.

Mechanical damage and natural corrosion have been identified as two of the largest causes of failures of gas pipelines (see Figure 2.5) [6]. Third party excavations and natural forces such as the movement of the earth deform the shape of the pipe, scrape away metal and cold work the steel [7]. Mechanical damage defects have been classified into three types, namely, gouges with metal loss, gouges with cold work and dents. The gouge with metal loss is a result of removal of metal from the pipe surface by an applied force. The remaining area of damage shows cold work. A forceful movement of metal in a local area on the pipe surface, resulting in wall thinning and cold working gives rise to what has been described as a gouge with cold work. A dent is a localized depression or deformation in the pipe's cylindrical geometry resulting from an applied force but without an associated gouge.

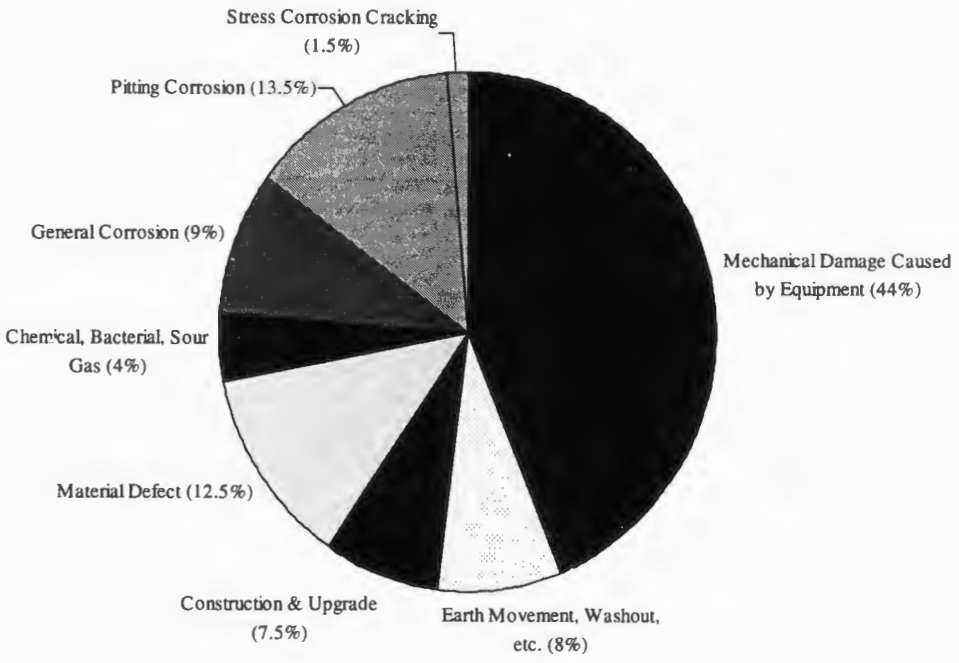

Figure 2.5. Incidents related to gas pipelines in USA [6].

The last few decades have seen a growing interest in "in-line" inspection procedures and NDE systems are being designed specifically for pipeline inspection. Today pipeline companies rely on state-of-the-art sensor technologies and advanced computation systems. Several different types of NDE methods have been tried and tested for inspecting pipelines. Ultrasonic and magnetic flux leakage techniques are among the most popular ones in use today.

Among the various techniques that can be used for the inspection of steels, magnetic methods are unique since they rely on the measurement of changes in the inherent ferromagnetic properties of the specimen and changes in magnetic properties are easily

measurable. Mechanical damage causes a local change in the geometric as well as ferromagnetic properties of the pipe, thus giving rise to local flux leakage. Consequently MFL tools are ideally suited to addressing the task of detecting mechanical damage [8].

Pipeline inspection is achieved in practice using a pipeline inspection vehicle, also called the "pig", which contains strong permanent magnets that magnetize the pipe wall axially as shown in Figure 2.6. The pig is conveyed through the pipes under the pressure of natural gas and a circumferential array of sensors measure the magnetic flux which leaks out in the vicinity of the defect. The leakage flux signal is digitized and stored on an "on-board" data acquisition system.

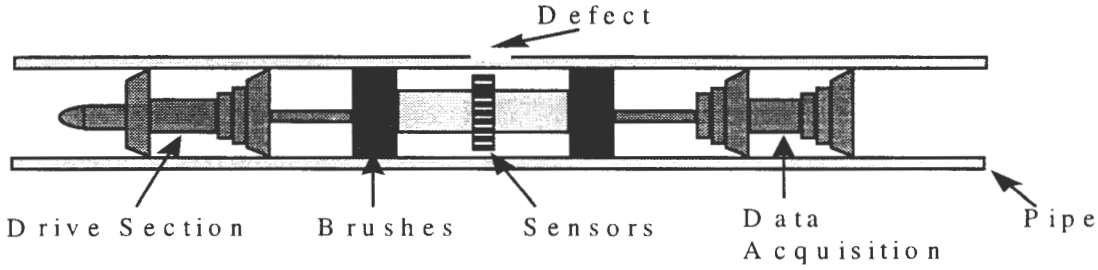

Figure 2.6. Pipeline inspection vehicle [9].

Each pigging operation generates a large amount of data (typically, 4 GB of compressed data for every 100 miles of pipe that is inspected), which is then systematically analyzed. A manual analysis and interpretation procedure is typically followed. It has however been found that the leakage field data is greatly affected by factors like permeability of the pipe material, velocity with which the pig is transmitted, thickness of the pipe wall etc [8]. This, along with the sheer volume of the data, makes manual signal analysis a tedious task. The recent years have therefore witnessed a growing interest in developing automatic

computer based analysis procedures. Work done at Iowa State University has led to the development of a three step procedure for analysis of MFL data [10]. The step procedure involves :

- **Signal Identification** - The MFL signal is generated at every region in the pipe where there is a local variation in the magnetic behavior. These include defects, welds, joints, T sections, valves, etc. The first step in analysis therefore involves identifying and separating the benign indications from the potentially hazardous ones.
- **Signal Compensation** - The MFL signal needs to be made invariant to changes in operational parameters like velocity of scan, permeability of the pipe, sensor location, etc.
- **Signal Characterization** - This step involves defect sizing and prediction of defect profiles from the MFL signal.

The above scheme of signal analysis can be represented as shown in Figure 2.7.

The ultimate goal of the signal analysis is detection and characterization of the defects. Very early research proved that the MFL signal topography could be used to distinguish between flaws in a specimen. Shcherbinin and Zatespin [10] showed that flaws like cracks could be approximated by magnetic dipoles. They performed experiments which generated leakage fields very similar to theoretical predictions generated using the magnetic dipole model. Their results indicated that the MFL signals were affected more by the defect depth than its width.

Defect characterization which can be cast as an inverse problem, has been a formidable research topic because of its ill-posed nature. Direct methods to solve the inverse

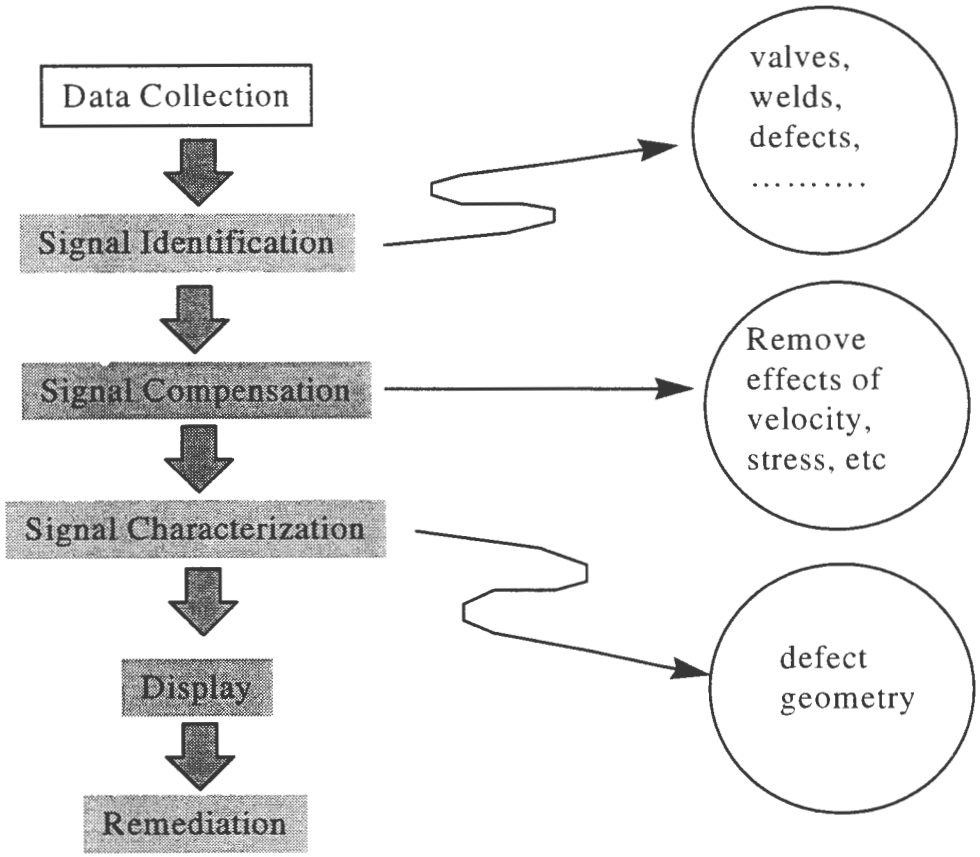

Figure 2.7. Steps in MFL signal analysis [10].

problem have had mixed results. Efforts are therefore being directed towards developing indirect methods. One of the earliest and most widely used approaches is the calibration method, where features in the measured data are compared to those derived from a set of standard signals obtained from known defects. Lord and Hwang [12] use finite element models to generate calibration curves linking defect parameters such as length, depth, width, etc. with specific signal characteristics. They also provide a systematic procedure for predicting defect parameters from the magnetostatic leakage flux signals. They found that the peak-to-peak value of the normal component of the leakage flux increased with increase in flaw depth, while the separation between peaks depended on the width of the flaw.

The flux leakage method has been compared with other NDE techniques with respect to its ability to characterize defects. Palanisamy and Curran [13] compared the performance of AC flux leakage and eddy current testing for sizing flaw depths in steel tubing. They found that the defect sizing accuracy of both techniques was more or less equal. However the AC flux leakage signal showed more oscillations than eddy current data. They also concluded that the AC leakage signal amplitude varied with defect depth as well as width in contrast to the eddy current signal amplitude which was affected only by the depth of the flaw.

The need for automated inspection of parts in the industry brought the microcomputer into the NDE process. Emphasis had been traditionally laid on improving electronics for transducers to detect the smallest defects and for analog signal processing. However with the advent of computers, digital signal processing was explored for the first time. Singh and Udpa [14] have studied the role that digital signal processing plays in NDT. They have described its application to defect detection and characterization.

Indirect methods for the solution of the inverse problem were developed using digital signal processing. Signal classification based methods which fall into this category rely on the ability to create a data bank of all expected defect types and corresponding signals [15]. Matched filters and feature-based pattern recognition methods using clustering algorithms or back-propagation neural networks are two types of classification techniques that are being widely used.

An automated crack detection system using magnetic particle testing was designed by General Motors for inspection of steel rods [16]. The system used computer vision and pattern recognition techniques to determine crack size and geometry. They processed the rods

through a magnetic particle solution and then presented it in front of a camera. The video image was digitized and fed into a microcomputer for analysis. Image processing techniques were used for detection of cracks. The system was capable of inspecting 1200 rods per hour.

More recently, neural approaches have been developed to obtain a direct and more complete solution to the inverse problem, in terms of reconstructing defect profiles. In general, the inverse problem can be described as an identification mapping f, from the measured 2D scan to the defect profile. This continuous valued mapping function f is approximated using function expansion techniques can be estimated using a radial basis function (RBF) network.

The use of RBF networks for defect sizing using MFL signals has been demonstrated [17]. Attempts have also been made to obtain a complete defect profile using finite element data and RBF neural networks [9][18]. Most characterization efforts have used only the axial component of the leakage field. This thesis describes an attempt to use both, the axial and the circumferential components of the leakage field. Work reported in this thesis is based on the premise that the circumferential component carries valuable information about the defect. Since current techniques utilize only the axial component, the use of the circumferential component in addition to the axial data is expected to provide an improvement in the quality of the predicted defect profile. A data fusion approach has been taken and neural networks have been employed to predict not just the length, width and depth of the defect, but a complete 3D defect profile. It is believed that such a characterization scheme provides added value to the pipeline inspection procedures and would lead to improved decision making for fault repair.

3. ARTIFICIAL NEURAL NETWORKS

3.1 Introduction

A neural network is in general, a collection of simple analog signal processors called neurons, that are densely interconnected through links called "synapses" [19]. The initial motivation underlying the development and study of the neural networks was to mimic the operation of the biological nervous system and implement a neural-like system on computers. One can regard a neural network to be a dynamic system (discrete or continuous), the states of which are the signals and the controls of which are the synaptic weights (which regulates the flow of the transmitters from one neuron to the other). Neural networks are of interest because of their inherent parallel nature and because they require no *a priori* information or rules. They acquire their "knowledge" through the presentation of examples. This is in contrast to modern day computers, which remain essentially serial in their operation and are not flexible in real time. A brief description of the biological neuron, which forms the basis of artificial neural networks, is presented here.

3.2 Neurons In The Brain

The computational element in the neural network (which is called the neuron), is appropriately named, as it attempts to emulate the neuron in the biological nervous system. This is a specialized cell which reacts to stimuli and communicates with neighboring neurons via fibers (connections) called axons and dendrites, as shown in Figure 3.1. The connection

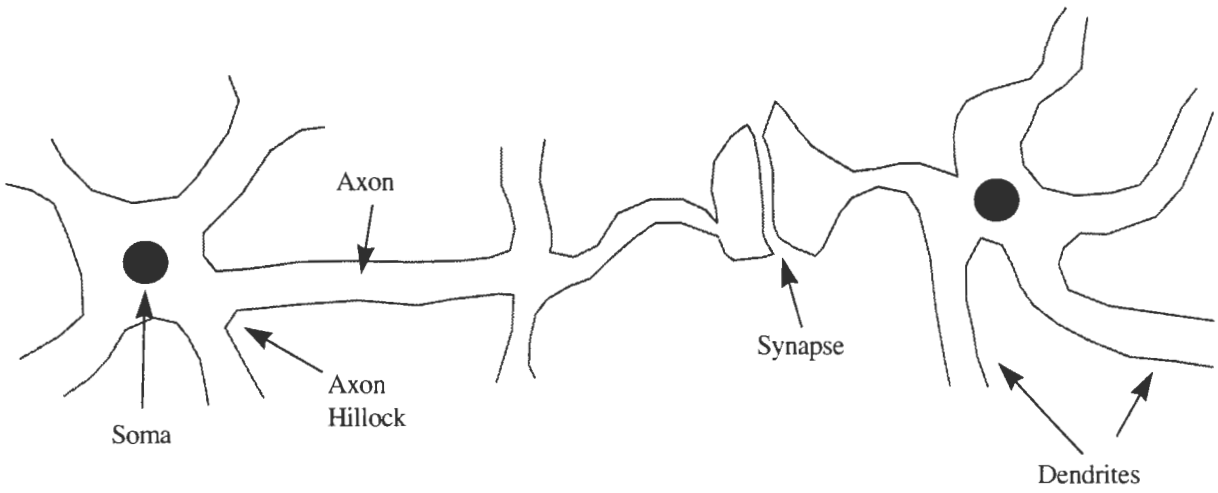

Figure 3.1. The biological neuron.

between the axon of one neuron and the dendrites of another is called a synapse. The neuron with its axon and dendrites is an independent processing unit.

The body of the neuron is made of chemical matter called soma. It generates large molecules which serve as transmitters and receptors. Communication between neurons takes place via a chemical ion-exchange process in the synapse. The sending synapse, when stimulated, releases neuro-transmitters which activate the gates in the dendrites. The gates are then opened, allowing the charged ions to travel up to the neuron body, thus altering its potential. Once a certain threshold is reached, the stimulated neuron generates it's response in the form of a spike which is called the 'action potential'. This spike travels along the axon to various synapses that the neuron is linked with. Thus, it is seen that some form of threshold logic is responsible for operation of the neurons.

3.3 Artificial Neural Networks

3.3.1 Historical Perspective

The artificial neural network has been based on a simplified model of the biological neuron. The first computational model of the neuron was proposed by McCulloch and Pitts [20], wherein they represented the neuron as a binary threshold unit, as shown in Figure 3.2. This unit integrated its many inputs and generated an output only if the integrated value exceeded a certain threshold. Several of these simple computational units were interconnected to form a simple network which was able to generate AND, OR, NOT, and NOR logic.

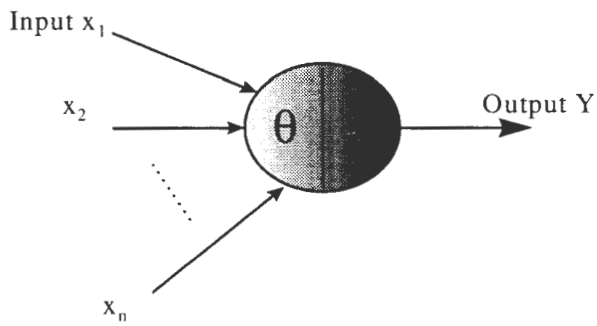

Figure 3.2. The McCulloch and Pitts neuron [19].

A more general computational model was proposed in 1958 by Rosenblatt. The major deviation from the binary unit, was the introduction of interconnection weights. Learning is achieved using a numerical algorithm to adapt the weights.

Rosenblatt's model was refined by Minsky and Papert [21], into the much used perceptron. The input to the perceptron is an n dimensional vector. It then performs a

weighted sum, adds a bias and passes the result through a non-linear element, as seen in Figure 3.3.

The perceptron can distinguish between classes separated by a linear decision boundary but fails to recognize a non-linear decision boundary. Its operation can be described by the following equations :

$$y = w^T x \qquad \ldots. 3.1$$

$$u = f_{HL}(y) \qquad \ldots. 3.2$$

where u is the output, x is the input vector, w^T is the transpose of the weight vector and the f_{HL} is the non-linearity, given by

$$f_{HL}(y) = \begin{cases} 1 & y > 0 \\ 0 & y < 0 \end{cases} \qquad \ldots. 3.3$$

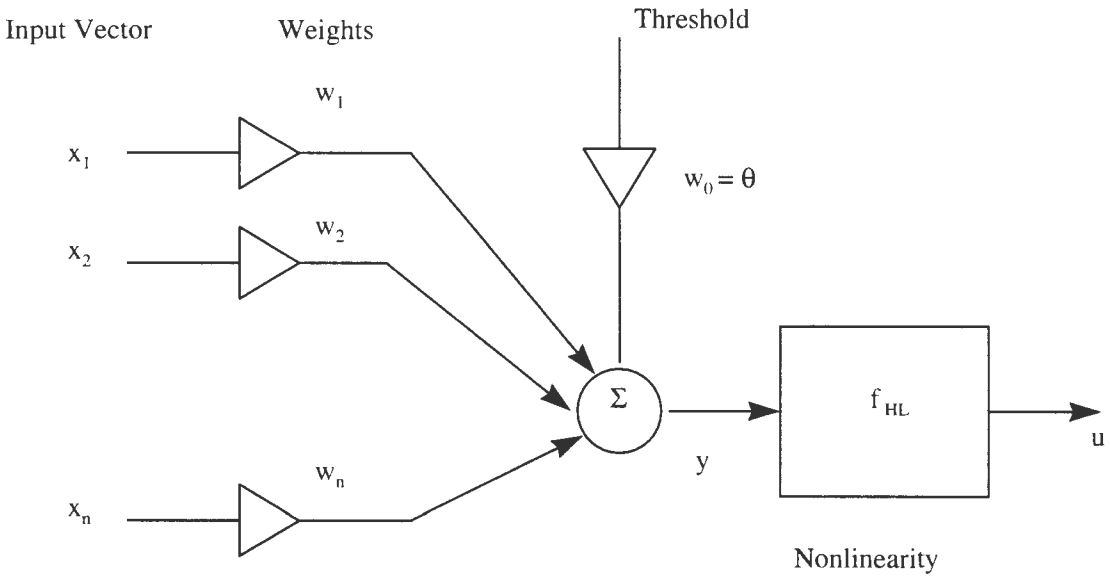

Figure 3.3. The perceptron [10].

The "Perceptron Learning Algorithm" deals with the problem of automatically determining the weights of the network so that it performs a specific task. A learning algorithm is therefore, an adaptive method by which a network of computing units self-organizes to implement the desired behavior. Two classes of learning algorithms are used: supervised and unsupervised. Supervised learning refers to the method in which learning is achieved by presenting some examples of the desired input-output mapping. A correction step is executed iteratively until the network learns to produce the desired output. A block diagram is shown in Figure 3.4. This method is used when the desired output is known. For applications in which the "ideal" desired output is unknown (e.g. pattern classification), unsupervised learning is used.

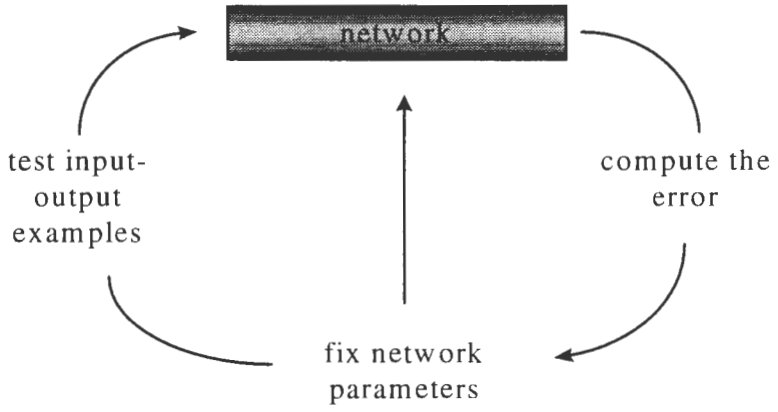

Figure 3.4. Supervised learning algorithm [25].

Neural network applications can be classified into two broad categories : *recognition* and *generalization.* The main distinction between these classes is that, in recognition problems, the network is trained with several inputs and is tested for its ability to reproduce the output corresponding to any of the inputs that it was trained with. Character recognition

problems fall into this category. Generalization problems test the capacity of a trained network to predict correctly the output corresponding to a new input signal, which the network has not encountered during its training phase. Many real-world problems which may be otherwise difficult to solve using mathematical techniques, benefit from the generalization capabilities of neural networks.

3.3.2 Common Network Architectures

- **Multi-Layer Perceptron (MLP)** - These are feed-forward networks with one or more layers of nodes between the input and the output. The MLP overcomes the limitations of a single perceptron, in that, it can generate arbitrary, complex, non-linear decision boundaries and can separate intermingled or meshed classes. This capability is obtained by using nodes that posses a nonlinear input/output relationship. A 4 layer perceptron with 2 hidden layers is shown in Figure 3.5.

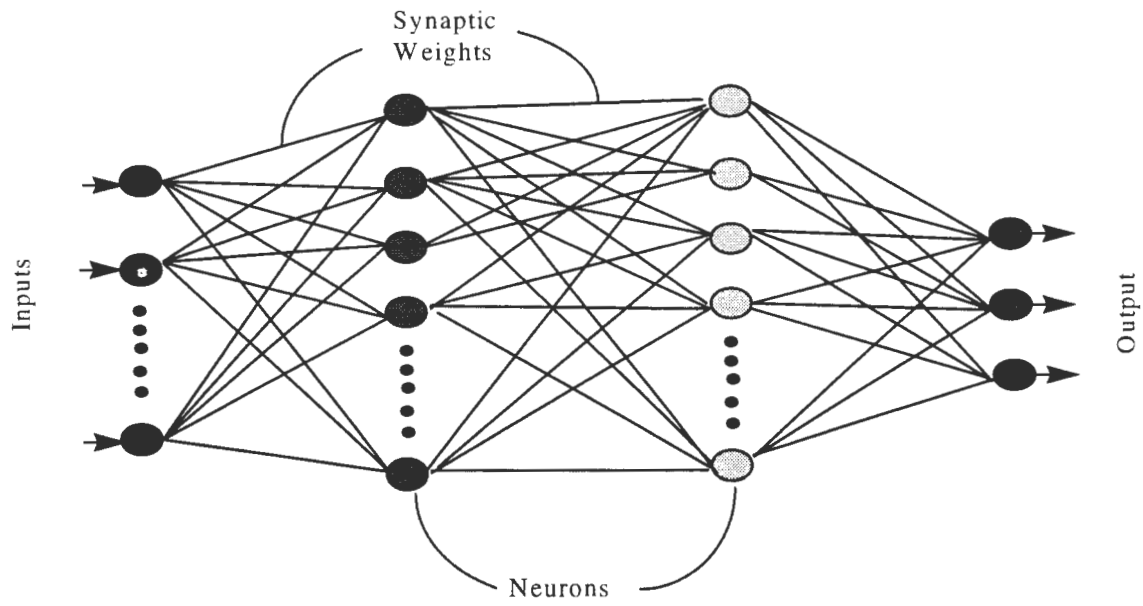

Figure 3.5. The Multi-Layer Perceptron (MLP) [9].

The MLP is usually trained with a supervised learning algorithm called the Backpropagation algorithm [22]. This is a gradient descent technique which is attempts to minimize an appropriate cost function. The MLP learns to generate a mapping from the input pattern space to the output pattern space, by minimizing the energy associated with the error between the actual output of the network and the desired output. The disadvantage of this technique comes with the fact that the backpropagation technique is basically a gradient search method which may get trapped in a local minimum instead of reaching the desired global minimum. In such a case, the algorithm may not converge to the globally optimal solution. Several adaptations have been proposed to overcome this problem and to speed up convergence [23].

- **Radial Basis Function (RBF) Neural Networks** - This type of network architecture can be considered as a hybrid, in that it combines/ couples the self-organizing network with a feed-forward network. The RBF network can also be considered as a multivariate interpolation technique [24], in which the learning process essentially involves determining a surface in a multidimensional space that provides the best fit to the training data. The architecture of the RBF network is shown in Figure 3.6 and is somewhat similar to that of the MLP, with the difference however, that it has only one hidden layer, while the MLP can have more. The nodes of the hidden layer provide a set of basis functions that produce localized stimulus to the input. The name "radial basis" comes from the fact that the kernels are radially symmetric.

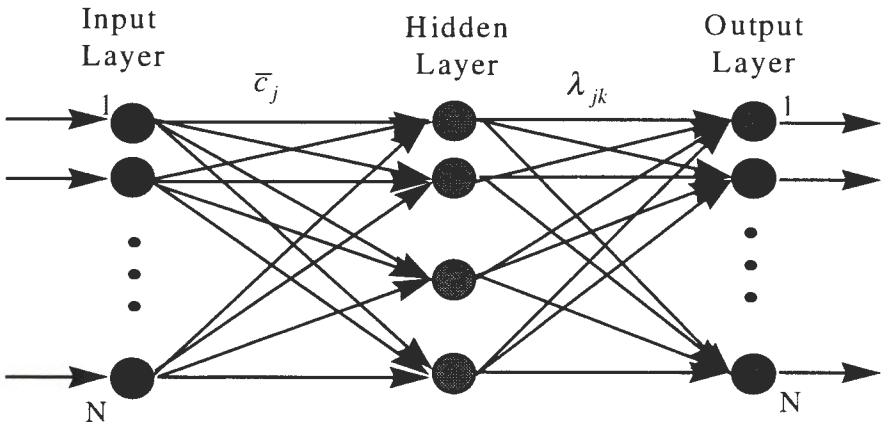

Figure 3.6. The RBF network [9].

Examples of radial basis functions include [25] :

1. Gaussian - $f(r) = e^{-r^2/\sigma^2}$
2. Multi-quadratic - $f(r) = (r^2 + \sigma^2)^{1/2}$
3. Inverse multi-quadratic - $f(r) = (r^2 + \sigma^2)^{-1/2}$
4. Thin plate spline - $f(r) = r^2 \log(r)$
5. Piece-wise linear - $f(r) = \frac{1}{2}(|r+1| - |r-1|)$
6. Cubic approximation - $f(r) = \frac{1}{2}(|r^3+1| - |r^3-1|)$

where, σ is a scaling parameter and r is the distance between the input vector and the center vector. The distance is measured using the Euclidean norm. The RBF network implements a multivariable functional interpolation scheme[24], based on the interpolation function *s(x)*, which maps the n-dimensional input space onto an m-

dimensional output space. This is accomplished by expanding $s(\underline{x})$ as a linear combination of the radial basis functions.

$$s(\underline{x}) = \sum_{j=1}^{m} \lambda_j \phi\left(\left\|\underline{x} - \underline{y_j}\right\|\right) \qquad \underline{x} \varepsilon \quad \Re^n \qquad \ldots. \ 3.4$$

where, $\phi\left(\left\|\underline{x} - \underline{y_j}\right\|\right)$ is the set of arbitrary basis functions, the vectors y_j are the centers of the basis functions and λ_js are the expansion coefficients which determine the nature of mapping that the function implements. The function $s(\underline{x})$ is chosen such that it satisfies the interpolation conditions

$$s(\underline{x}) = f_i \,. \qquad i = 1,2,..m \qquad \ldots. \ 3.5$$

which implies that the function is constrained to pass through the known data points. Inserting these interpolation conditions into Equation 3.4, a set of linear equations for the coefficients $\{\lambda_j\}$ are obtained.

$$\begin{pmatrix} f_1 \\ . \\ . \\ f_m \end{pmatrix} = \begin{pmatrix} A_{1\,1} & . & . & A_{1m} \\ . & . & & \\ . & & . & \\ A_{m1} & & & A_{m\,m} \end{pmatrix} \begin{pmatrix} \lambda_1 \\ . \\ . \\ \lambda_m \end{pmatrix} \qquad \ldots. \ 3.6$$

where, A_{ij} is defined as $\phi\left(\left\|\underline{x} - \underline{y_j}\right\|\right)$. Thus, if matrix A is invertible and the centers y_j are known, the expansion coefficients can be uniquely obtained as $\lambda_j = A^{-1} f$. The coefficients λ_j appear linearly in the expansion for the radial basis functions. Matrix A has a unique inverse, provided it is non-singular. It has been shown that for a large choice of the basis functions $\phi(.)$ and a set of distinct data points, matrix A is indeed non- singular.

The training of an RBF network consists of three steps : (a) determining the basis function centers (b) determining the support of the basis functions and (c) computing the interconnection weights. Several algorithms have been developed for selecting the centers. Some of these are described in the following paragraphs.

3.3.3 Algorithms for RBF Center Selection

- **K-means Clustering -** is a simple method for determining the centers of basis functions by classifying sets of data into clusters based on their "proximity". The algorithm [26] minimizes a cost function consisting of the sum of squared distances from all points in a cluster domain to the cluster center. The clustering result depends heavily on the number of clusters and the initial choice of cluster centers. This algorithm has been used in this study and is described in detail in Chapter 4.
- **Potential Functions Approach** - This is a self-organizing and iterative center selection method [25]. It integrates an overall error fit between the predicted and the true sample values. Consider applying this method to determine the decision function between two classes. This method views the sample patterns as a source of energy. The potential at any one sample point reaches a peak and then gradually decreases away from the point. Pattern classes can be represented as "plateaus" formed by all the patterns at peaks of a group of hills. The classes are separated by a "valley" where the potential is essentially zero. The potential function for any input sample can be characterized by the expression

$$K(x, x_k) = \sum_{i=1}^{\infty} \lambda_i^2 \varphi_i(x) \varphi_i(x_k) \qquad \ldots. \ 3.7$$

where, $\varphi_i(x)$, i = 1, 2, … are assumed to be orthonormal and λ_i, i = 1, 2, .. are real numbers different from zero chosen such that the potential function $K(\mathbf{x},\mathbf{x}_k)$ is bounded for $\mathbf{x}_k \in \omega_1 \cup \omega_2$. Equation 3.5 represents the general form of the potential function. Two basic types of functions that fit the above general form may be used while implementing the algorithm. The first one, referred to as potential functions of Type 1 is a truncated series of the form

$$K(x, x_k) = \sum_{i=1}^{m} \varphi_i(x)\varphi_i(x_k) \quad \ldots. 3.8$$

Potential functions of Type 2 are symmetrical functions of the two variables $\mathbf{x}$ and $\mathbf{x}_k$. An example of Type 2 functions is given below :

$$K(x, x_k) = \exp\left\{-\alpha \|x - x_k\|^2\right\} \quad \ldots. 3.9$$

The decision function $d(\mathbf{x})$ can be constructed from a sequence of potential functions $K(\mathbf{x},\mathbf{x}_1)$, $K(\mathbf{x},\mathbf{x}_2)$, etc. and is related to the potential functions by the set of orthonormal functions $\varphi_i(x)$. The cumulative potential is the aggregate of the individual potentials. The input signals are presented to the algorithm in sequence and at each step, a cumulative potential is calculated. If this value is less than a pre-established threshold, then a new center is formed. The process continues till the cumulative potential calculated at each of the input patterns is less than the threshold.

- **Conjugate Gradient Descent Algorithm** - This method, also known as the Fletcher-Reeves method [27] , is a modification of the steepest descent algorithm. It involves minimization of a cost function subject to the constraint that each new search direction is conjugate to the previous one.

The first step involves setting up of a cost function, which could be expressed as

$$E = \frac{1}{2} \sum \lambda_i e_j^2 \quad \text{.... 3.10}$$

The summation is over all the training samples and e_j is the error defined as

$$e_j = d_j - \sum \lambda_j \phi \left(\| \underline{x} - \underline{y_j} \| \right) \quad \text{.... 3.11}$$

where, $\phi\left(\|\underline{x} - \underline{y_j}\|\right)$ as explained earlier, is the set of basis functions.

It has been shown that any minimization procedure that uses conjugate directions is quadratically convergent [28]. This property ensures that the method will minimize a quadratic function in n steps or less. To understand the concept of conjugate directions, consider the problem of finding a minimum value of the quadratic function f(x) = ½**X**'G**X** + b'**X** + c, where G is a positive, definite and symmetric matrix. In two dimensions, the curves f(x) = K, for different values of K are concentric ellipses, as shown in Figure 3.7. Suppose that in a search for a minimum from point A in direction AD, the minimum occurs at point B and C is the optimal point, then direction BC is said to be conjugate to AD. This idea can be extended to n dimensions.

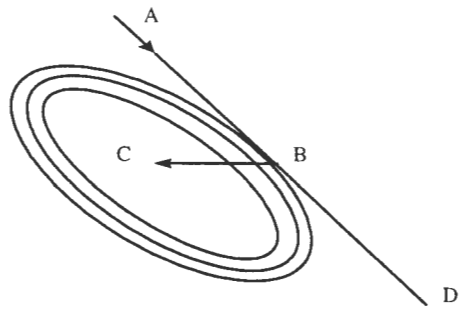

Figure 3.7. Conjugate directions.

An algorithm to determine centers minimizes a cost function f(x) using the above rule involves the following steps :

1. Start with an arbitrary initial point X_1.
2. Set the first direction $S_1 = - \nabla f(X_1) = - \nabla f_1$.
3. Find point X_2 according to the relation $X_2 = X_1 + \lambda_1 S_1$, where λ_1 is the optimal strength in direction S_1. Set i = 2.
4. Find $\nabla f_i = \nabla f(X_i)$ and set $S_i = - \nabla f_i + (| \nabla f_i |^2 / | \nabla f_{i-1} |^2) S_{i-1}$.
5. Compute optimum step length λ_i in direction S_i and find new point $X_{i+1} = X_i + \lambda_i S_i$.
6. Check with preset error criterion and stop if X_{i+1} is optimal. Else repeat steps 4 and 5.

This method is used to determine the optimal centers, support and coefficients of the basis functions simultaneously.

- **Spectral Mapping - Simulated Annealing Approach** - This, in contrast to all the above algorithms, is not a position-domain method. Spectral mapping uses the spectrum of the input and output signals. This enables considerable data reduction as most of the information contained in the signals is represented by a few low frequency components. This results in reduced complexity and training times of the neural network. The spectrum is obtained by taking the Fast Fourier Transform (FFT) of the signals. Simulated annealing is a process used for global optimization and is a modification of the gradient descent technique. In this case, it is used to determine the RBF parameters by minimizing a cost function. Annealing in condensed matter physics, is the thermal process for obtaining low energy states of a solid in a heat bath [29]. The physical annealing process is modeled using computer simulation methods, by assuming an analogy between a

physical many-particle system and a combinatorial optimization problem. A parameter called the control parameter (which represents the temperature) is introduced and the cost function is evaluated at decreasing values of the control parameter. A typical feature of the simulated annealing algorithm is that besides improvements in cost, it allows to a limited extent, temporary deterioration in the cost. This feature enables the algorithm to escape from local minima unlike the local search algorithms. It however still exhibits the simplicity and applicability of local search algorithms.

The algorithms for training RBF networks are guaranteed to converge since there is only a single layer of adjustable weights which may be evaluated according to linear optimization techniques.

4. DATA FUSION

4.1 Introduction

The concept of data fusion is a not a very new one. However, its application to the field of NDE is fairly recent. Data fusion is a deceptively simple concept which is enormously difficult to implement. Fusion refers to the synergistic combination of information made available by various sources/ sensors, in order to provide a better understanding of the scene. A distinction has been made between multisensor integration and multisensor fusion. Multisensor integration, as defined by Luo and Kay [30], refers to the systematic use of the information provided by multiple sensory devices to assist in the accomplishment of a task by a system. The notion of multisensor fusion is a more restricted one, in that it refers to any stage in the integration process where there is an actual combination (or fusion) of different sources of sensory information into one representational format. A general pattern of multisensor integration and fusion can be represented as in Figure 4.1.

The concept of data fusion can be understood perfectly well by comparing it with human brain. Humans have five main sensory organs and fusion of information by occurs every time the senses are activated by appropriate signals. For example, the sound of a voice captured by the ear and the visual information captured by the eye helps the brain in identifying a person. Interesting examples of human and other animal data fusion have been discussed by Luo and Kay [31] in their review of data fusion.

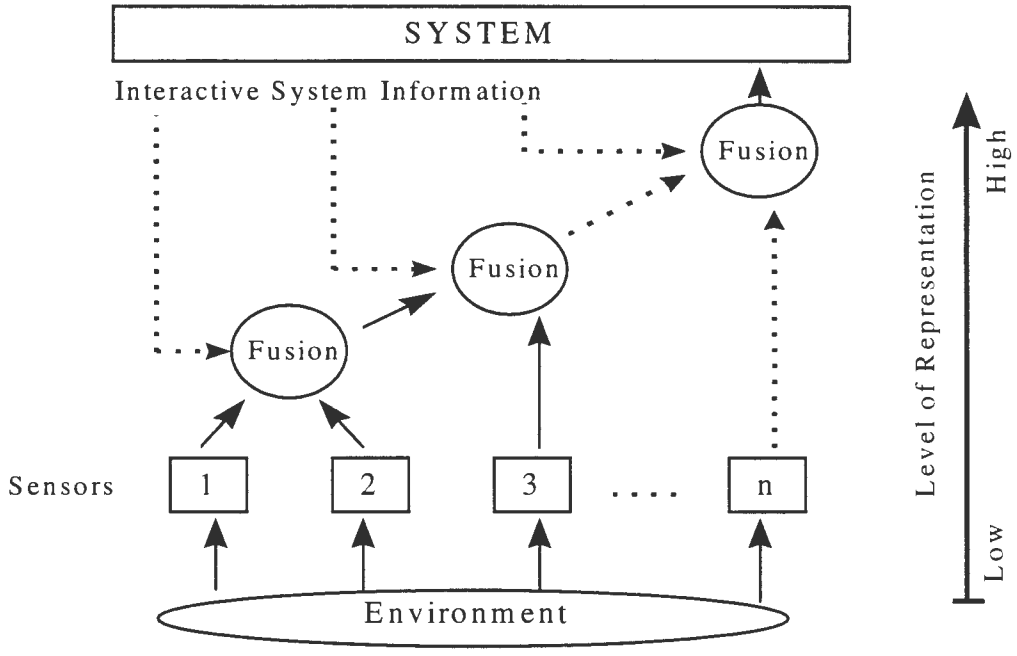

Figure 4.1. A general pattern of multisensor integration and fusion [30].

Data fusion algorithms can be categorized into two types, viz. phenomenological algorithms which take into account the effects of the underlying physical processes while fusing the data and non-phenomenological algorithms which ignore the underlying physical processes. These can be further classified into algorithms that bring about fusion at the signal, pixel, feature or at the symbol level. Signal level fusion (which has been implemented in this work) is applicable when sensors have identical or similar characteristics or when the relation between the sensors is known. Pixel level fusion is used to fuse images. Feature level fusion is the one in which a reduced data set (termed as the feature set) representing the original signal, is used for fusing the data. The highest level of fusion is symbol level fusion where abstract elements called symbols are used for fusion.

Fusion is not very simple to achieve. Several problems have been identified with respect to the fusion process [31]. Problems result from errors during sensor operation (e.g. calibration), sensor failure, coupling among components of the integrated system and due to the control necessary to co-ordinate the operation of the various sensors.

4.2 Data Fusion Paradigms and Models

Several different approaches to fusion have been studied and suggested over the years. Luo and Lin [32] have suggested a hierarchical phase-template approach as a general paradigm for multisensor integration in robotic systems. They have identified four distinct temporal phases in the sensory information acquisition process, distinguished by the range over which sensing takes place, the subset of sensors required and the type of information desired. The information acquired at each phase is represented in the form of a template and the data collected by each sensor is recorded as an instance of that phase's template. These templates are later fused into one.

A "logical sensor" approach has been proposed [33] as a specification for the abstract definition of a sensor. Through the use of this abstract definition, unnecessary details relating to the actual physical sensor are separated from their functional use in a system. This is similar to abstract data types used in device drivers and more recently in object oriented programming. The use of logical sensors can provide any multiple sensor system with portability and the ability to adapt to technological changes in a manner transparent to the system.

A more recent paradigm deals with the use of neural networks for sensor integration and fusion. As seen earlier in chapter 3, neural networks are an attempt to mimic the function

of the nervous system and the human brain is probably the best analogy to the concept of data fusion. It is thus evident that neural networks would be naturally suited to the task of fusion. Artificial neural networks would typically be used for signal level fusion. One of the very early attempts at using neural networks for fusion was made by Pearson et al. [34], who presented a neural network fusion model based on the design of the visual/ acoustic target localization system of the barn owl. They used neuronal maps which are large arrays of locally interconnected neurons that represent information in a map-like form. The neuronal maps are key building blocks of the nervous system function.

Eggers and Khuon [35] present a neural network data fusion decision system for detection and classification of space object maneuvers simultaneously observed by two radars of different aspect, frequency and resolution. They use a statistically based adaptive preprocessor for each sensor and a highly parallel neural network for associating the outputs of the preprocessors to the appropriate decisions.

Feature level fusion has also been achieved using a hierarchical neural architecture [36]. In hierarchical networks, the neurons at higher levels are insensitive to noise, distortion and scaling at the lower levels. The activities of the higher level neurons in networks processing different sensor data have thereby been combined to achieve fusion at feature level.

Neural networks have also been used in NDT data fusion applications. NDT images obtained from different inspection techniques like eddy current and ultrasonic techniques have been fused to obtain an image that is optimal in the least squares sense[37]. Neural networks have been used in automated inspection systems that employ data fusion concepts

[38]. A neural network has been used, for example, in tube inspection systems as a classifier. The automated classifier was able to distinguish between defects and the support features of the tube.

Other models [31] used for fusion include the Kalman filter which is used for dynamic low level fusion of redundant data, the Bayesian estimation theory whose central idea is to first eliminate any sensor information that might be in error and then fuse the rest of the data, the statistical decision theory which is a two step process used to fuse redundant location data from multiple sensors and the Dempster- Shafer evidential reasoning theory which has been used in military applications for target recognition. Recent efforts have also been directed towards the use of fuzzy logic for scene analysis and object recognition.

An in-depth study of data fusion as applied to NDT has been made by Gros [39]. A description of the various NDT methods and fusion techniques has been provided. The application of the Bayesian and the Dempster-Shafer theory to eddy current data fusion has been explained in detail. Fusion has been achieved for data from multiple sensors to combine quantitative defect information such as depth, length, etc. Applications of NDT data fusion that have been studied, have shown that fusion can be performed using data which is as close as possible to the original data. Thus the loss of information which might occur due to excessive processing is minimized and the burden of complex operations is reduced. Fusion can easily be applied to different types of inspections regardless of sensor types. However, the particular technique used for fusion depends on the type of defects and the equipment used for inspection. Multisensor data fusion thus is a worthwhile endeavor to increase the efficiency of a nondestructive evaluation process.

4.3 Fusion Of MFL Data

While fusing information from various sensors, attention needs to be paid to the "registration" of the data from these sensors. This implies that the various sensors must make their measurements on the system at exactly the same time (temporal registration) and/ or under the same spatial conditions (spatial registration). Spatial registration is especially important when images are to be fused.

In the present study, 3 sets of sensors record the three components of the MFL signal. Fusion has been attempted at the signal level to combine information from two sensors, viz. the axial and the circumferential sensors. Temporal registration has been ensured, which means that the signals have been recorded at exactly the same instant of time.

It was observed from the MFL signals obtained for the different defect types used in the study that, the axial and the circumferential signals vary to a considerable extent from defect to defect. The variation in the signals from the circumferential sensors was observed to be much greater than that from the axial sensors. While the axial signals showed only an increase in magnitude with increase in defect depth, the circumferential signal changed considerably, with respect to the placement of the "lobes" and their relative sizes. It is therefore inferred that the circumferential component may be related to the defect shape and would provide additional information in the characterization process. An attempt was made to fuse the data from these two sensors, to obtain a combined signal which would represent the axial and circumferential components and also carry information not revealed by the components individually.

Data fusion was accomplished in agreement with the physical nature of the two components. As mentioned in chapter 2, the axial component is measured in a direction parallel to the flaw, while the circumferential signal is measured perpendicular to the flaw. The two signals are thus mutually orthogonal. Taking this fact into account, fusion is achieved by considering the two components as the real and imaginary parts of a complex number. Thus a single measure (the magnitude of the complex number) for data from both the sensors is made available.

4.4 Feature Extraction

Since the fused MFL signal for each defect is represented in the form of a complex matrix, the amount of data to be handled is large. In order to optimize the neural network architecture and training time, the neural network needs to be presented with a concise input data set. Feature extraction therefore becomes essential.

Feature extraction has been performed using the Principal Component Analysis (PCA). This is a technique for forming new variables which are linear composites of the original variables [40]. Geometrically, it involves projection of the variables onto a new set of axes that make a certain angle with the present axes. There is precisely one such angle that results in a new variable accounting for maximum variance in the data. The new axes are called principal components and the values of the variables are called principal component scores. PCA is used as a dimensional reducing technique, i.e. instead of using all of the p original variables to represent the data, m linear combinations (principal component scores) are used, where m may be much less than p. Typically, the sum of the variances of the new variables not used to represent the data is used as a measure for the loss of information

resulting from representing the data in a lower dimensional space. The linear combinations are designed so that the first new variable accounts for the maximum variance in the data, the second one accounts for the maximum variance that, has not been accounted for by the first new variable, and so on. Thus, all the new variables are mutually uncorrelated and all PCs together account for 100% of the variation in the data.

Principal components have been determined by taking the eigen vectors of the covariance matrix of the data, in this case, the fused complex matrix. Data reduction is achieved by retaining only a few of the PCs depending on how much data loss can be tolerated in the application at hand. The numerical eigen values give an indication of the amount of information carried by the respective principal component. For the MFL data set, it was observed that the first eigen value of the covariance matrix was much higher than the rest and that the eigen values decayed rapidly The average condition number for the data matrices was to the order of 10^8. The ratio of the first eigen value to the second one was observed to be very large (average ratio = 20) which indicates that the first principal component carried most of the significant information in the signal and the data loss occurring if all other PCs were ignored, would be tolerable. It was therefore decided to use the first principal component scores as the feature vector to represent fused axial and circumferential components of the MFL signal. Considerable data reduction was thus achieved. Code for the feature extraction was written in MATLAB.

4.5 K-means Clustering

K-means clustering is a process for partitioning an N-dimensional population into K sets, on the basis of a sample and has been shown to result in partitions efficient with respect

to within class variance. It has been used in the present work to determine centers of the basis functions for the neural network. The K-means procedure is easily programmed and is computationally efficient. It has therefore been widely used to process large number of samples on a digital computer. Extensive research has also been carried out to investigate optimization techniques for this algorithm.

The K-means procedure could be viewed as a process starting with K groups each of which contains a single random point initially and thereafter adding each new point in the population to the group whose mean is nearest to the point. After a point is added to a group, the mean of that group is adjusted to take into account the new point. Therefore at any stage, the K means are the means of the K groups. The process of assigning points whose centers are closest continues until convergence is obtained. This is equivalent to minimizing a performance index defined by the sum of squared distances from all points in a cluster domain to the cluster center. A general convergence proof for the K-means procedure does not exist but a detailed study of the convergence behavior of this procedure has been made [40]. There are some cases in which the algorithm will converge while there are others where it will not. The algorithm has been shown to converge when the data can be partitioned into clusters that are linearly separable [25].

The performance of a defect characterization neural network using RBFs depends heavily on the choice of centers for the basis functions. Clustering algorithms are among the mostly commonly used approaches for center selection. The Gaussian function centered at c_i and defined as $\phi\left(x - c_i^{\,2}\right) = exp\left(-\left\|x - c_i\right\|^2\right)$, has been used in this study, as the radial basis function for the RBF neural network. The K-means clustering algorithm has been used

to determine the centers of the RBFs. Implementation of the algorithm involves the following steps [25] :

1. Choose K initial cluster centers $c_1(1)$, $c_2(2)$, ... $c_m(m)$. These are arbitrary and the first K samples from the given data set are usually selected.
2. At the k^{th} iterative step, distribute the training samples, {x}among the K cluster domains, using the relation,

$$x \in X_j(k) \quad if \quad \|x - c_j(k)\| < \|x - c_i(k)\| \qquad \text{.... 4.1}$$

for all $i = 1, 2, \ldots, m$, $i \neq j$, where $X_j(k)$ denotes the set of samples whose cluster center is $c_j(k)$.

3. Compute the new cluster centers $c_j(k+1)$, $j = 1, 2, \ldots m$ as follows :

$$c_j(k+1) = \frac{1}{M_j} \sum_{x \in X_j} x(k) \qquad \text{.... 4.2}$$

The new center is chosen such that the sum of squared distances from all points in $X_j(k)$ to the new center is minimized.

4. The algorithm is deemed to have converged and the procedure is terminated if $c_j(k+1) = c_i(k)$, for $j = 1, 2, \ldots, m$. Otherwise, go to Step 3.

The behavior and performance of the K-means algorithm is influenced by the number of clusters chosen, the choice of initial centers and the order in which the data is presented to the algorithm. In practice, experimenting is required with different values of K and different starting data configurations.

Once the centers have been selected, the expansion coefficients for the network can be determined using shown in section 3.3.2 (Equation 3.6), thus completely defining the

multivariate mapping. The RBF network can then be trained. The K-means algorithm was implemented using MATLAB. Code was also written for the training and testing of the neural network.

5. RESULTS AND CONCLUSIONS

5.1 Approach

The objective of the research work described in this thesis is to predict a complete 3D defect profile of mechanical damage defects occurring in gas pipelines. An RBF neural network was selected to be used for the characterizing the defect. The MFL data used in this research was obtained experimentally. An algorithm to fuse the information contained in the axial and circumferential components of the MFL signals was then designed. After pre-processing and data fusion, feature extraction was performed to reduce the size of the input data. An RBF neural network was then trained to predict defect profiles. The network was first trained using a part of the experimental data. The trained network was then tested for its ability to predict defect profiles when new MFL signals (i.e. a signals which are not a part of the training data set) are presented. Details of the experiment and the neural network characterization procedure are provided in the following sections.

5.2 Mechanical Damage Experiment

5.2.1 Introduction

The inspection of gas pipelines is a technically challenging and a very expensive task, requiring state-of-the-art technology. The expensive nature of a typical test run makes it difficult to obtain experimental data. Unfortunately, defect characterization schemes employing neural networks require an extensive data set both for training as well as testing. In order to generate a reasonably large data set, experiments were conducted by the Materials

Characterization Research Group at Iowa State University. This "in-house" experiment was aimed toward obtaining MFL signals for mechanical damage defects. Defects shapes were carefully chosen to mimic those encountered in real pipelines. Samples of these defects were made on steel plates and MFL signals were obtained.

5.2.2 Sample Preparation

The first set of defects are cup-shaped mechanical damage defects (gouges). Figure 5.1 shows the technique used to make these defects. All the defects were made on 4"x1/4"x16" , 1018 cold finished flat steel plates. The gouges were made by pressing a steel ball bearing on the steel plate, using a hydraulic pressured machine. Two different size ball bearings and ten pressure levels were used to obtain a total of twenty gouge defects.

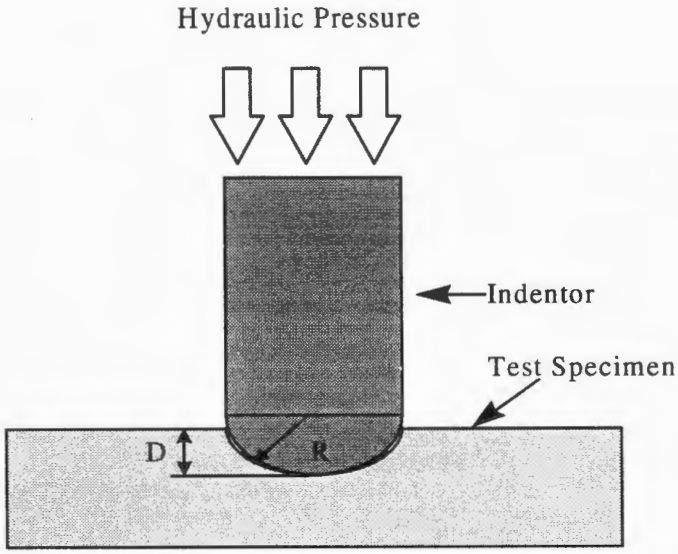

Figure 5.1. Fabrication of mechanical damage (cup-shaped) defects.

Only two defects were produced on each plate, so as to avoid the effects of "blooming" that occur when the defects are very near each other, causing the magnetic fields to overlap.

In order to test the ability of the neural network to predict profiles for different defect shapes, "V" (or wedge) shaped defects were also made. A special kind of indentor was designed in order to make these defects. A piece of steel in the shape of a "V" with a 90^0 angle between the arms of the V was fastened to a base of the same kind of steel (see Figure 5.2). Special care was taken to see that the indentor was securely fastened and did not move sideways on the specimen. Once again, a hydraulic machine was employed to generate the 10 different pressure levels to obtain ten V-shaped defects. These were made on steel plates that are identical to those used for producing the cup-shaped gouges. Table 5.1 gives a summary of the entire defect set along with the labels used to identify the defects in this thesis. The defect dimensions as measured using a micrometer are given in Table 5.2 and Table 5.3.

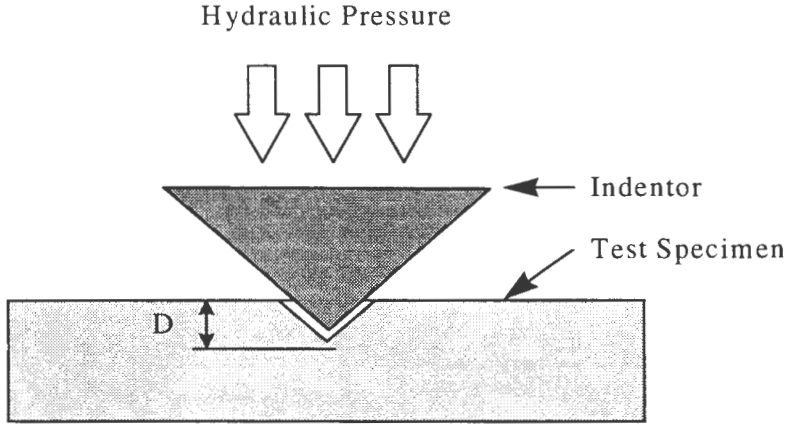

Figure 5.2. Fabrication of mechanical damage (V-shaped) defects.

Table 5.1. Experimental defect set.

Indentor Shape	Pressure Levels (thousands of pounds)									
	10	20	25	30	35	40	45	50	55	60
5/8" cup shape	A1	A2	A3	A4	A5	A6	A7	A8	A9	A10
1" cup shape	B1	B2	B3	B4	B5	B6	B7	B8	B9	B10
V shape	C1	C2	C3	C4	C5	C6	C7	C8	C9	C10

Table 5.2. Defect dimensions - cup shaped defects.

Defect	Diameter (inches)	Depth (inches)	Defect	Diameter (inches)	Depth (inches)
A1	0.201	0.0166	B1	0.211	0.0112
A2	0.285	0.0344	B2	0.295	0.0222
A3	0.331	0.0473	B3	0.339	0.0296
A4	0.346	0.0523	B4	0.366	0.0347
A5	0.386	0.0668	B5	0.393	0.0402
A6	0.400	0.0724	B6	0.415	0.0451
A7	0.436	0.0884	B7	0.432	0.0491
A8	0.449	0.0951	B8	0.470	0.0510
A9	0.484	0.1149	B9	0.483	0.0621
A10	0.500	0.1250	B10	0.510	0.0699

Table 5.3. Defect dimensions - V-shaped defects.

Defect	Depth (inches)	Defect	Depth (inches)
C1	0.0195	C6	0.0775
C2	0.0345	C7	0.0820
C3	0.0468	C8	0.0880
C4	0.0545	C9	0.0949
C5	0.0635	C10	0.1065

5.2.3 Experimental Setup

The experimental setup included a magnetization system and a data acquisition system. The magnetization system consisted of a magnetizer, also called the yoke and a controlled current source. The yoke consists of ferromagnetic blocks arranged to form a "U" shaped object that is about 24" long, 12" high, and 4" wide. Figure 5.3 shows a simplified diagram of the setup. The material used for the yoke is high permeability 1018 steel whose carbon percentage varies approximately from 0.15-0.23 %. The yoke is wound with a 550 turn coil using AWA copper wire. The test specimens were magnetized to saturation levels using excitation current values up to 50 amperes corresponding to magnetization levels of 34,400 A/m. The data acquisition system included a Hall probe connected to a Gaussmeter which was used to detect and measure the three components of the leakage field from the defect. The Gaussmeter was connected to a microcomputer containing an A/D converter. Data representing each component is stored in matrix form. MFL data was obtained for the entire defect set.

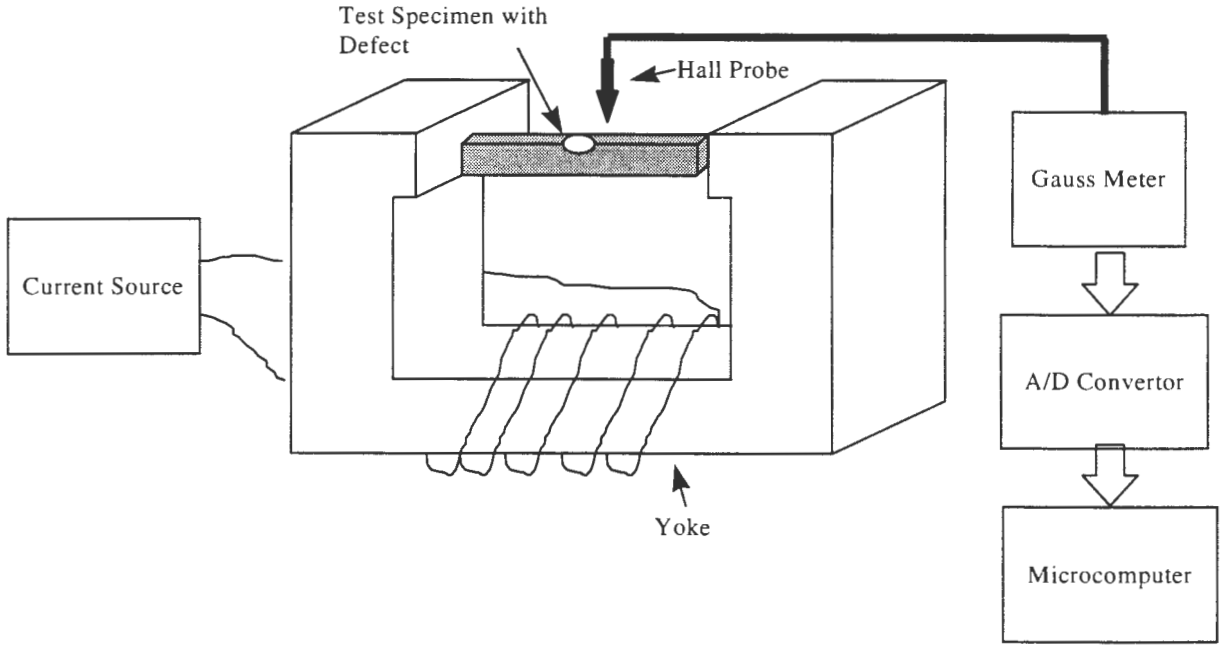

Figure 5.3. Experimental setup.

5.3 Results

A careful selection of training and test data was made for the neural network. It was observed that the signals from the defects made using 10 klbs[1]. pressure were extremely weak and had to be excluded from the study. The neural network was first trained to recognize and predict profiles for spherical defects. The signals from the cup shaped defects, for pressure levels 20, 30, 40, 50 and 60 klbs. were used as training data and those from the intermediate pressure levels, viz. 25, 35, 45 and 55 klbs. were used as test data as shown in Table 5.4 and Table 5.5.

Thus a total of 10 training data points were used and the performance of the network was tested using 8 test data points.

Table 5.4. Training data set - spherical defects.

Indentor Shape	Pressure Levels (thousands of pounds)				
	20	30	40	50	60
5/8" cup shape	A2	A4	A6	A8	A10
1" cup shape	B2	B4	B6	B8	B10

Table 5.5. Test data set - spherical defects.

Indentor Shape	Pressure Levels (thousands of pounds)			
	25	35	45	55
5/8" cup shape	A3	A5	A7	A9
1" cup shape	B3	B5	B7	B9

profiles were predicted as shown in Figure 5.4. It is noteworthy that the small differences in the MFL signals for spherical defects with different diameters where picked up by the neural network and were effectively used to characterize the signals.

The next step involved design of a generalized neural network which would be able to characterize MFL signals from various kinds of defects. For this purpose, an extended training data set was used wherein the MFL signals from the V-shaped defect were also included.

[1] klbs = kilo-pounds

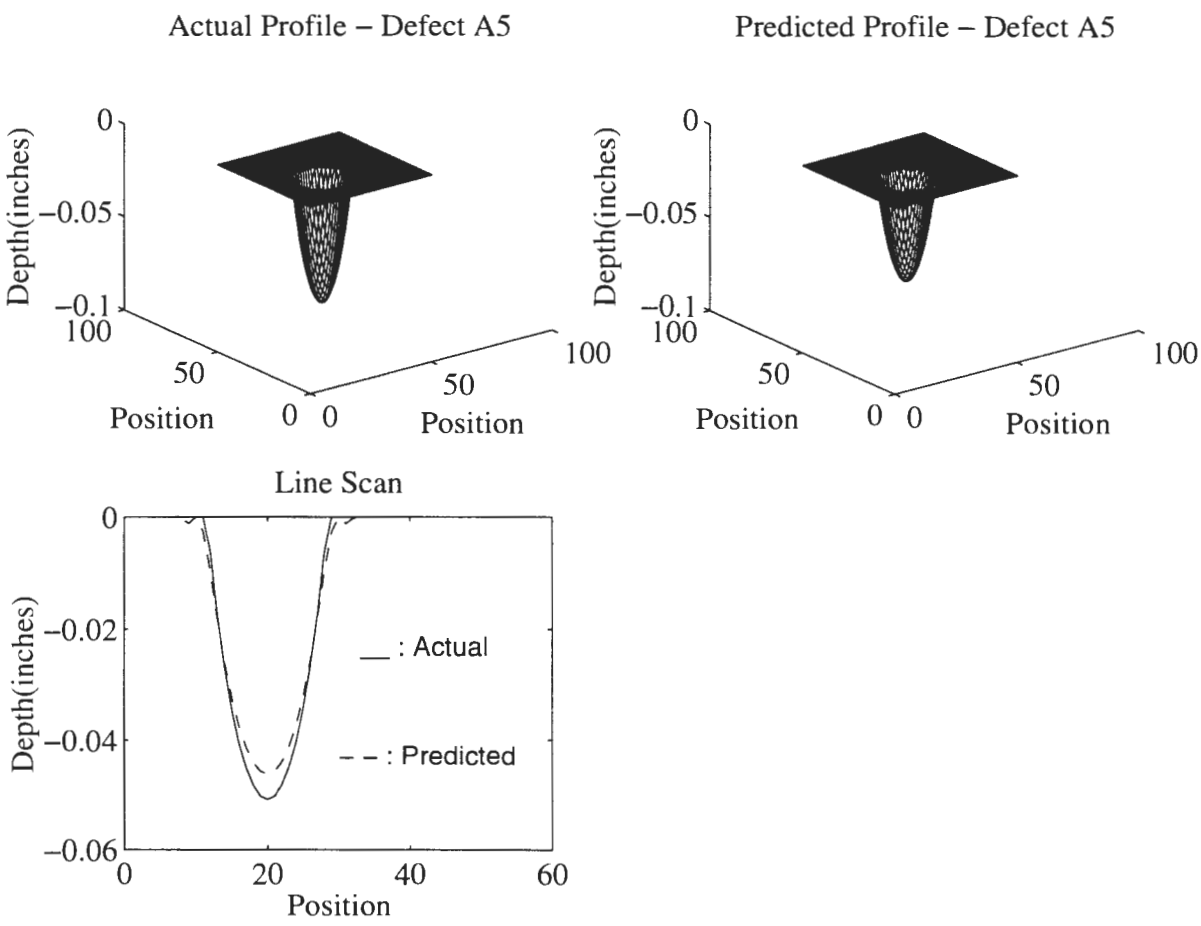

Figure 5.4. Results - spherical defects. (a) Defect A5.

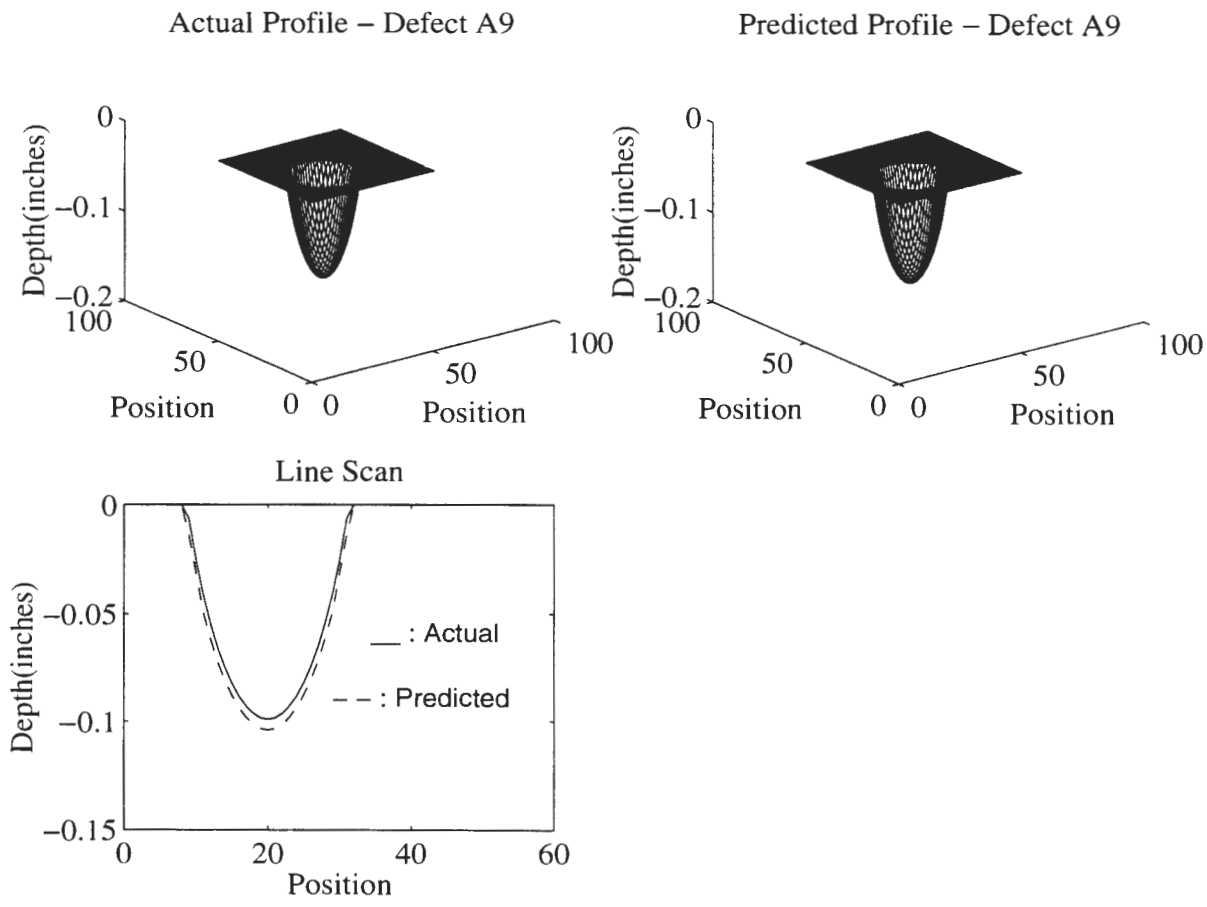

Figure 5.4. (continued) (b) Defect A9.

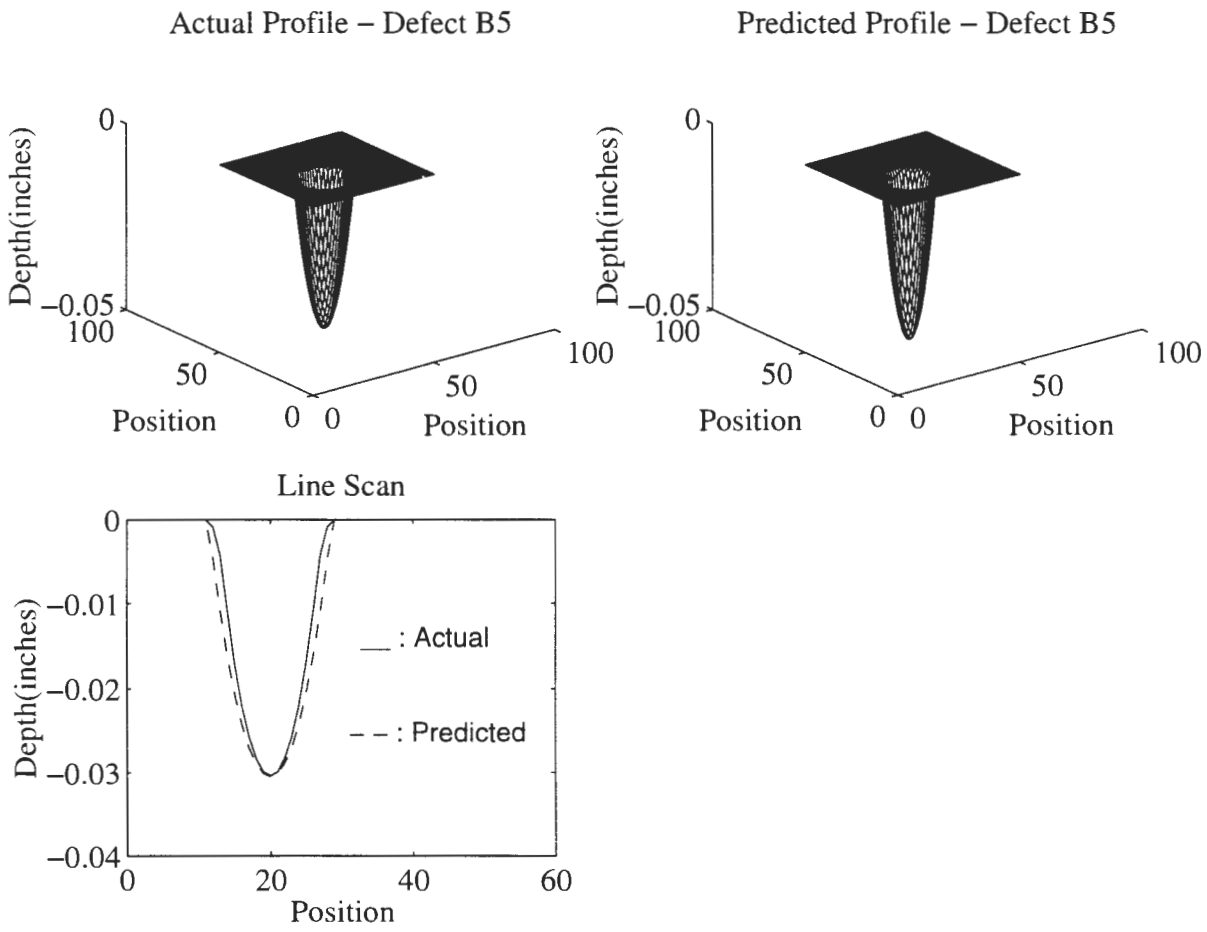

Figure 5.4. (continued) (c) Defect B5.

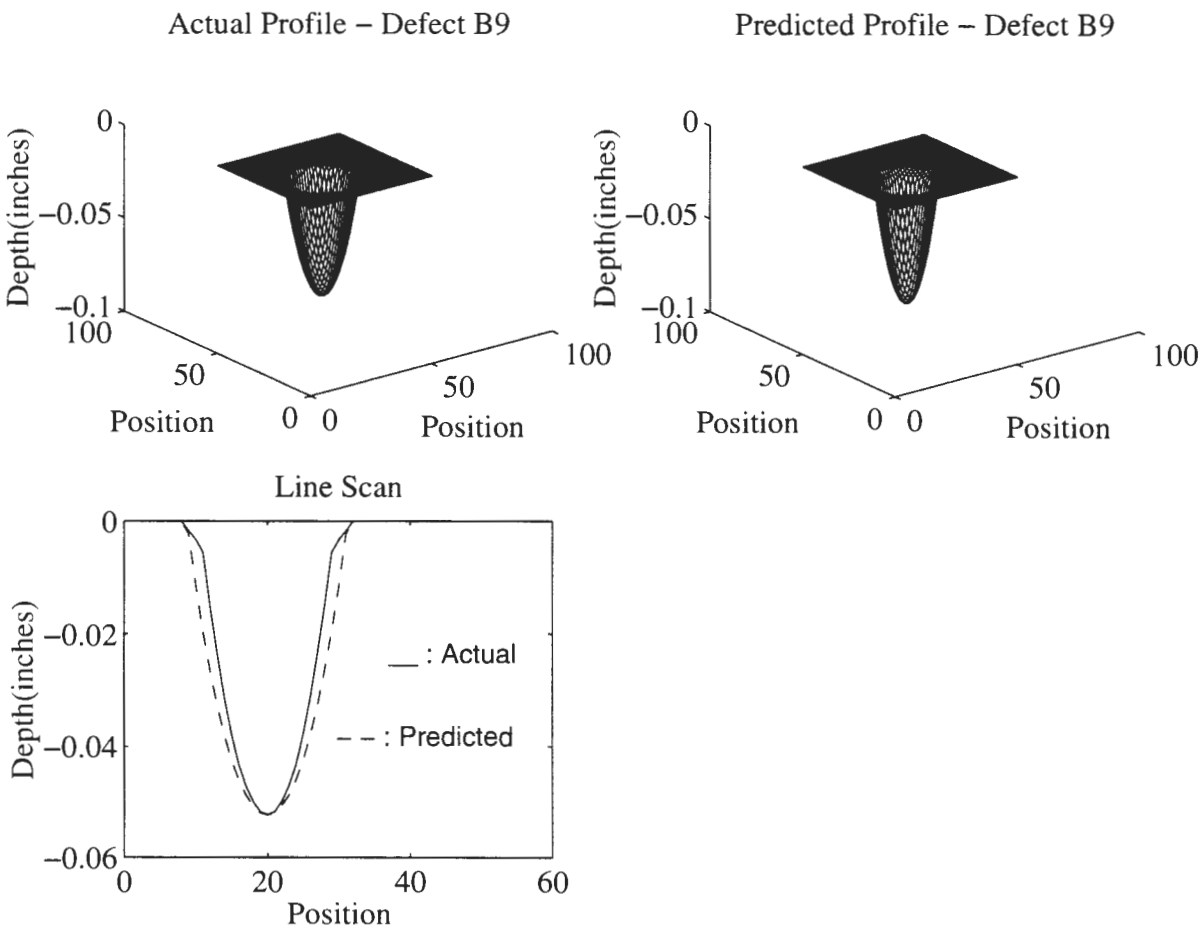

Figure 5.4. (continued) (d) Defect B9.

The extended training and test data sets are given in Table 5.6 and Table 5.7. It should be noted that the defect shapes used in this study are extremely different from each other and test the neural networks' generalization capability to the fullest extent. Also, the V-shaped defect with sharp edges presented a discontinuity to the network. Inspite of these harsh conditions, a considerable accuracy in profile prediction was achieved, as seen in Figure 5.5.

Table 5.6. Extended training data set.

Indentor Shape	Pressure Levels (thousands of pounds)				
	20	30	40	50	60
5/8" cup shape	A2	A4	A6	A8	A10
1" cup shape	B2	B4	B6	B8	B10
V shape	C2	C4	C6	C8	C10

Table 5.7. Extended test data set.

Indentor Shape	Pressure Levels (thousands of pounds)			
	25	35	45	55
5/8" cup shape	A3	A5	A7	A9
1" cup shape	B3	B5	B7	B9
V shape	C3	C5	C7	C9

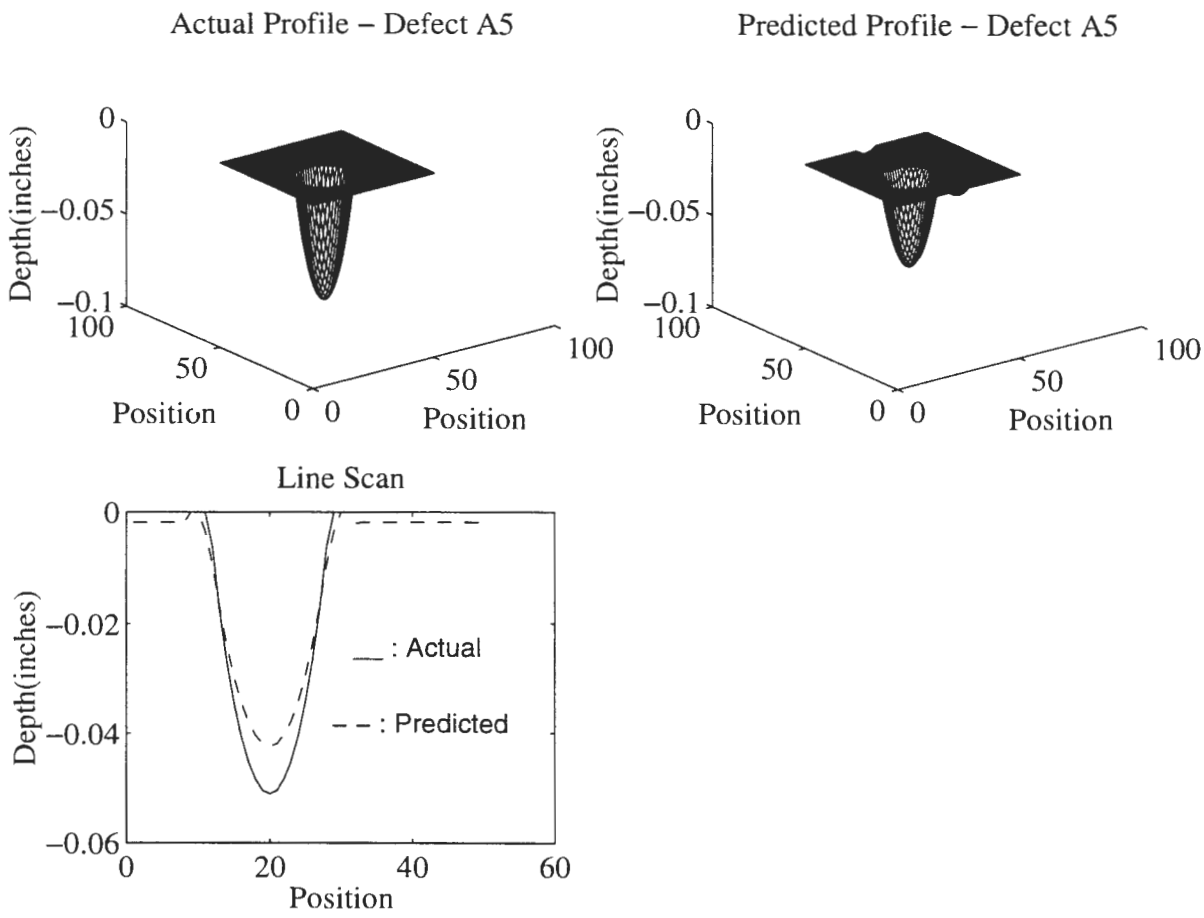

Figure 5.5. Results - different defect shapes. (a) Defect A5.

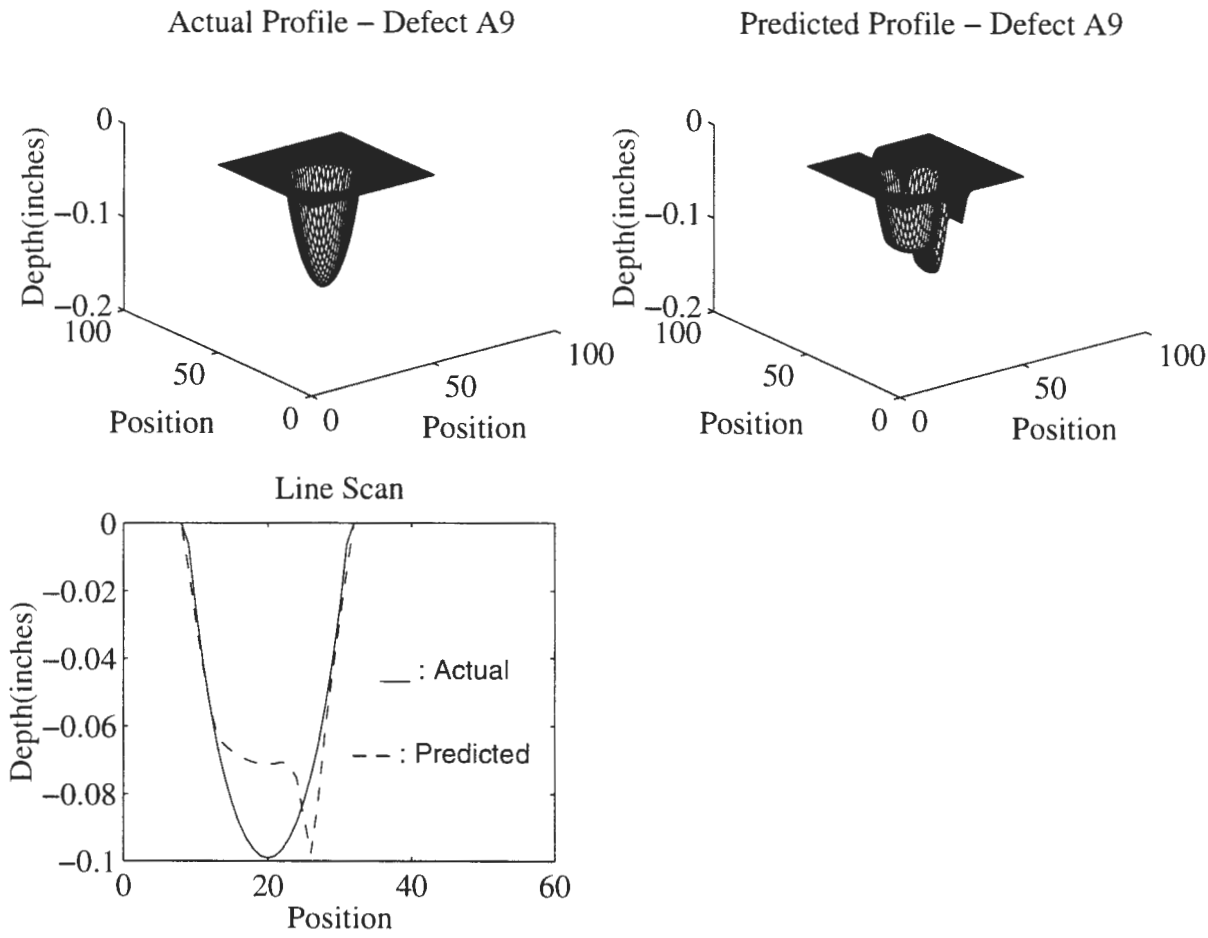

Figure 5.5. (continued) (b) Defect A9

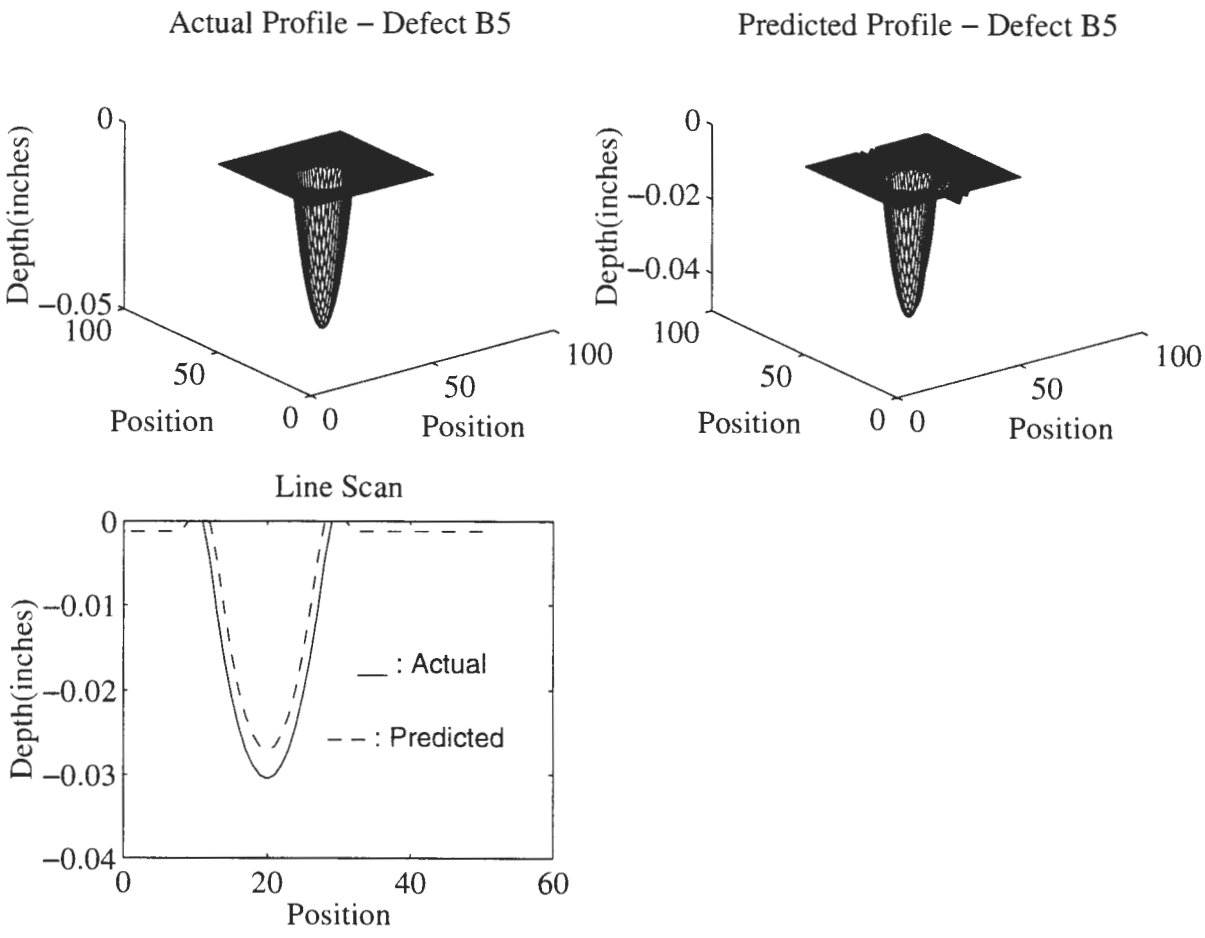

Figure 5.5. (continued) (c) Defect B5.

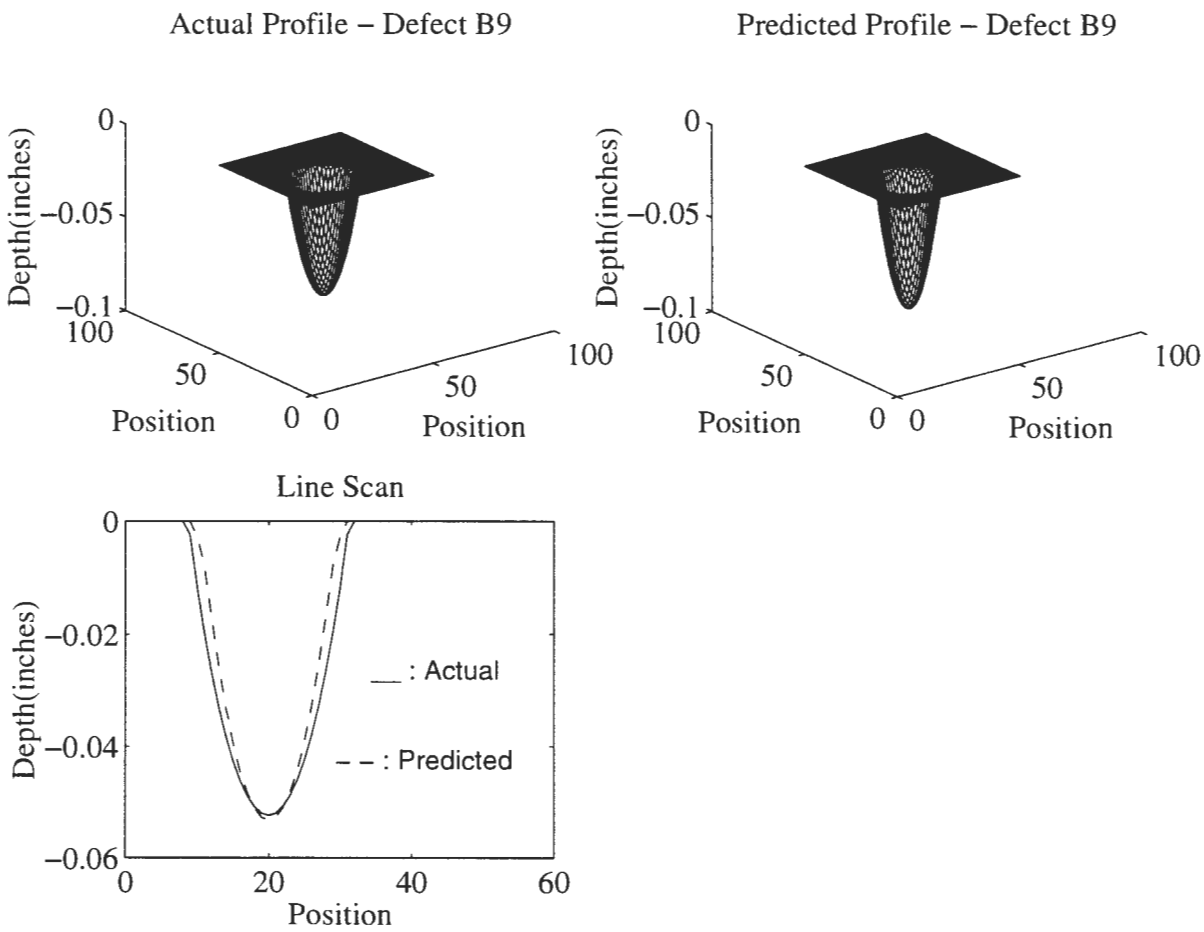

Figure 5.5. (continued) (d) Defect B9.

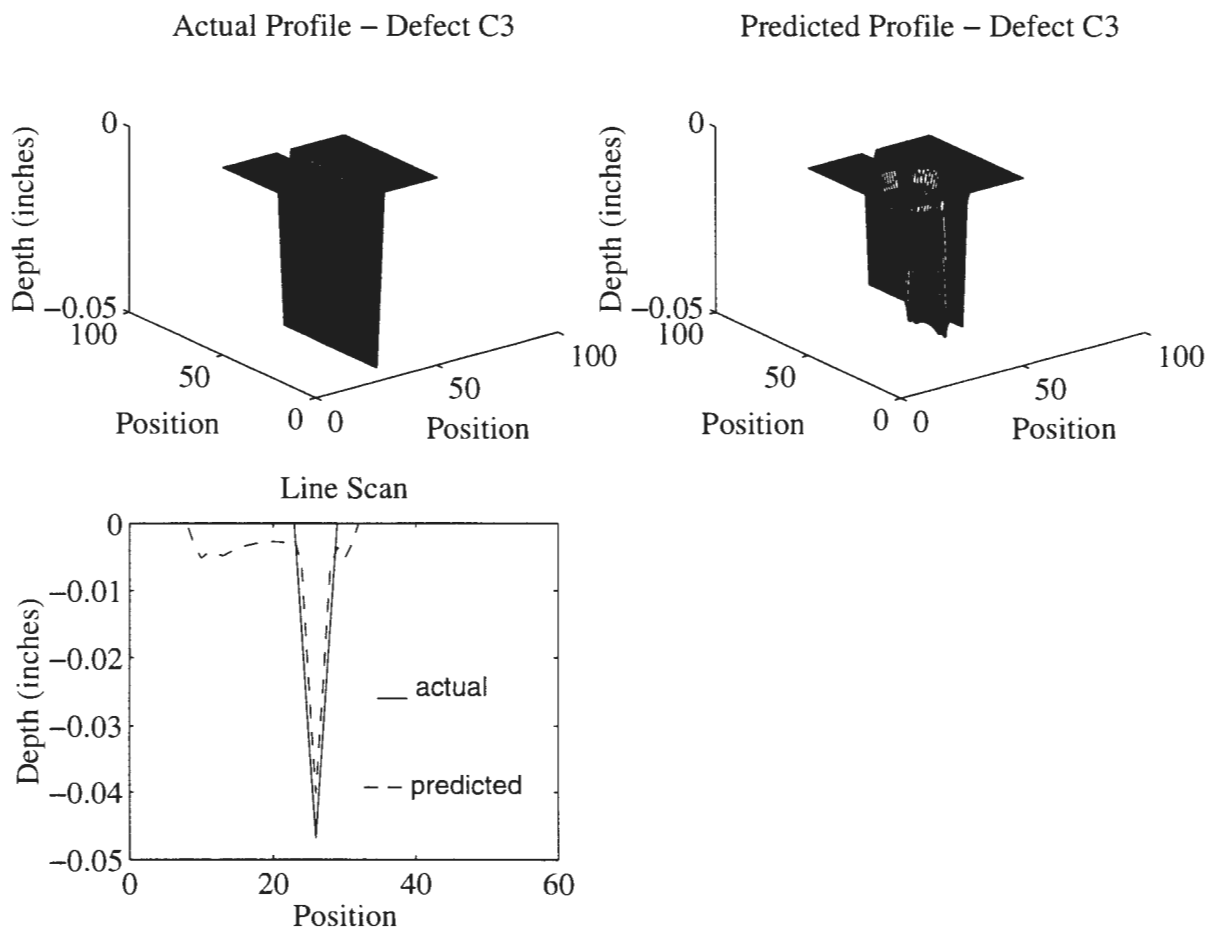

Figure 5.5. (continued) (e) Defect C3.

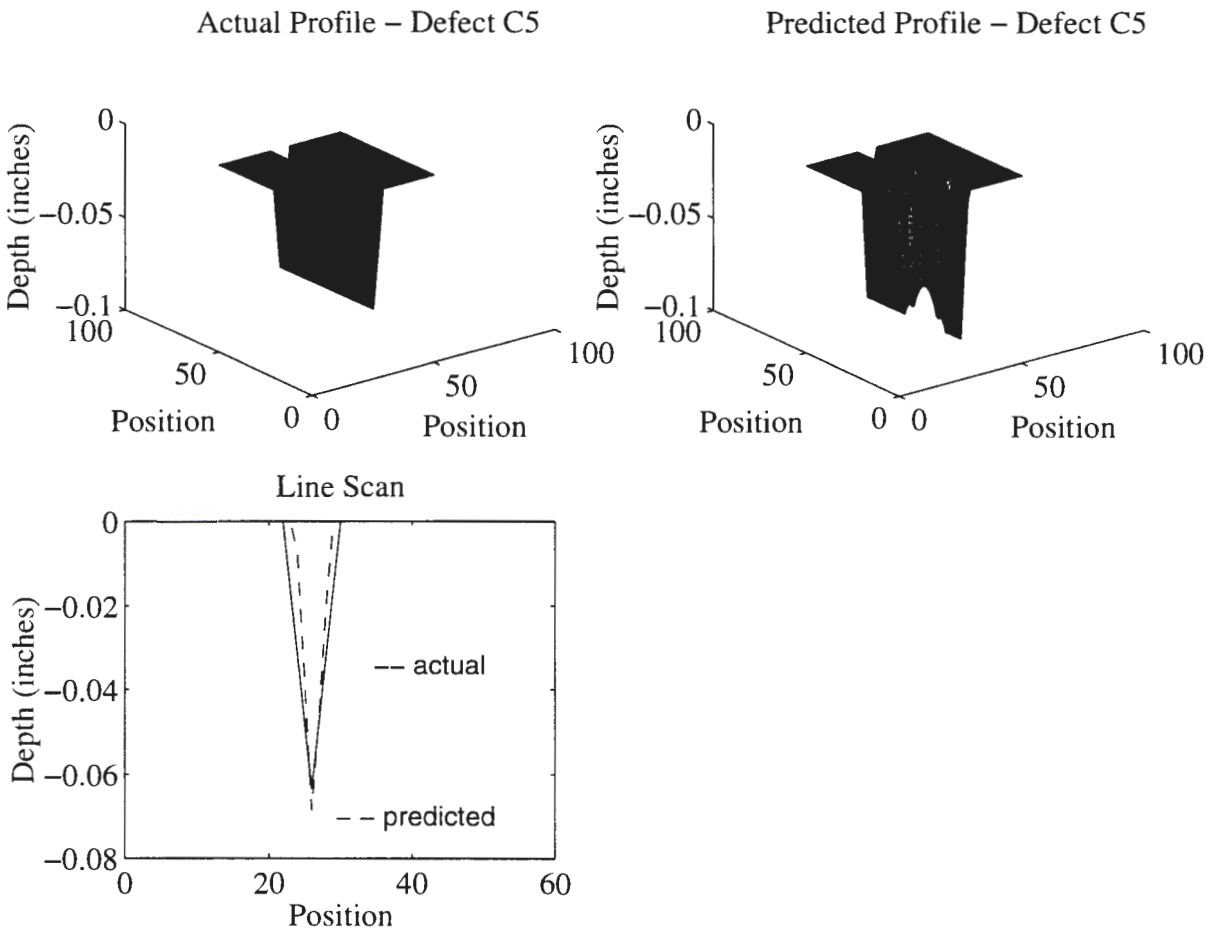

Figure 5.5. (continued) (f) Defect C5.

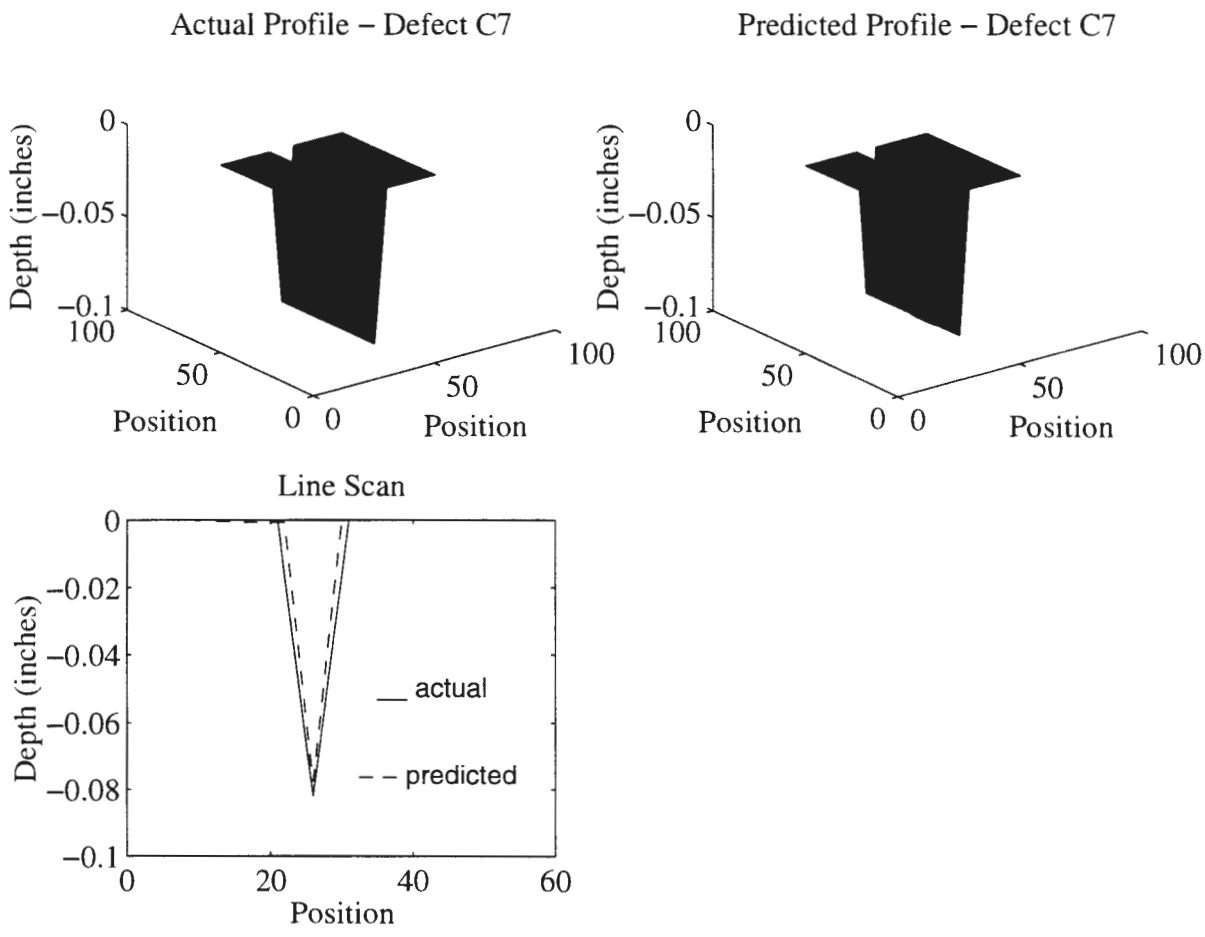

Figure 5.5. (continued) (g) Defect C7.

Performance evaluation tests were conducted for the neural network by varying the number of training data samples used and the order in which they were presented to the network. It was observed that if the number of training samples from each defect category was reduced, the performance of the network deteriorated. This shows that higher the amount of training data, better the results from the neural network. The order in which the training samples were presented to the network also changed the profile predictions. Best results were obtained if the training samples were arranged approximately in the order of defect depth. Tests were also conducted to determine the optimal support and optimal number of centers for the radial basis functions. Since an optimization algorithm was not used, a trial and error procedure was followed to determine the number of centers that would yield the most accurate predictions.

Tests were also conducted to evaluate the improvement in defect profile prediction due to data fusion. A similar neural network was trained using identical number of training data samples and identical support for the radial basis functions, but using just the axial component of the MFL signal as the input, instead of the fused complex matrix. It was found that the predictions from the neural network were fairly accurate with respect to the relative depths of the defects, however the performance suffered in the shape predictions. The comparison between predictions obtained with and without using data fusion is show in Figure 5.6.

5.4 Summary and Conclusions

The performance of the MFL technique for prediction of defect profiles was evaluated. The task at hand involved inspection of natural gas transmission pipelines for

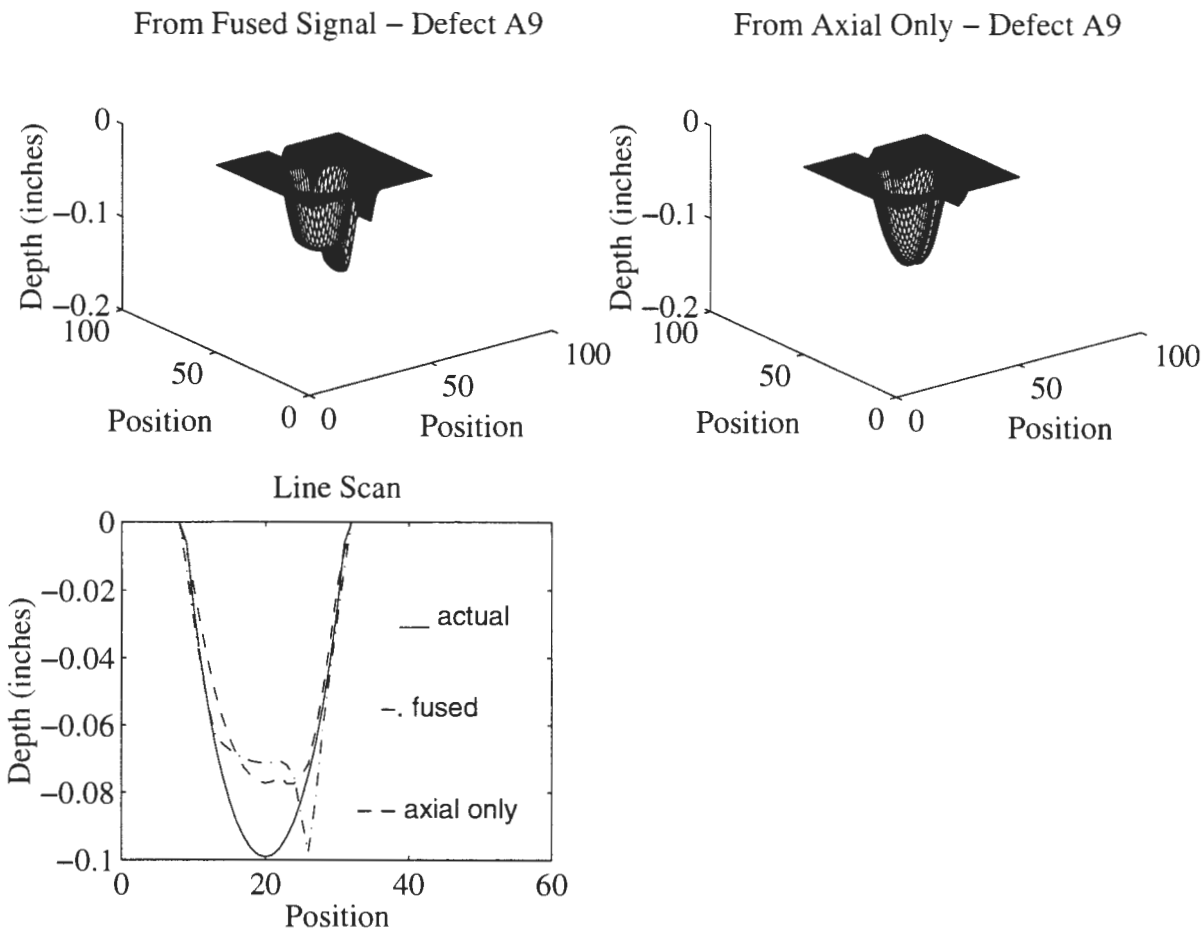

Figure 5.6. Comparison between predictions. (a) Defect A9.

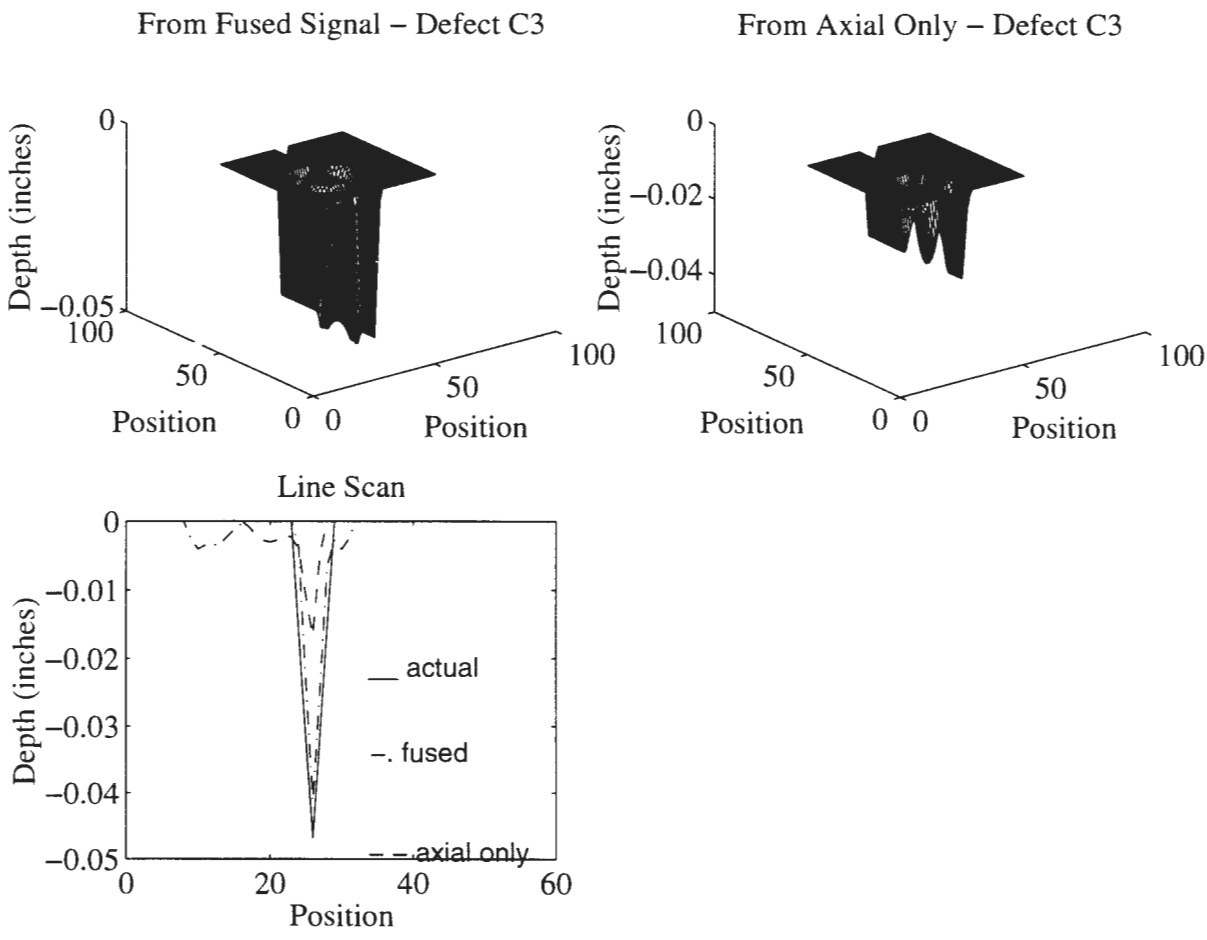

Figure 5.6. (continued) (b) Defect C3.

defects which might hamper the integrity of the pipes. A special category of defects, viz. mechanical damage defects were studied. The objective of the work was to predict complete 3D profiles of defects using neural networks for characterization. A data fusion approach was taken wherein, signals corresponding to the axial and circumferential components of the MFL signals were combined to obtain a fused measure of the leakage field.

An "in-house" experiment was designed and conducted to obtain experimental data. An RBF neural network was trained using the K-means clustering algorithm for center selection. Defect profiles were predicted for 3 different defect shapes and results obtained were presented.

The results validated once again, the feasibility of using the leakage field measurements for predicting defect profiles. Fairly good accuracy with an average mean square error of only 0.0037 was obtained and a neural network capable of predicting profiles for different defect shapes was made available. The results were compared with those from earlier efforts [41] which used only the axial component of the leakage field. It was found that the profiles obtained in the present study were more accurate with respect to the defect shape and internal surface. Tests conducted using the present approach and data also confirmed that data fusion yielded more accurate predictions. Thus the use of the circumferential component has been justified.

The small inaccuracies in the defect profiles predicted by the generalized network can be attributed to the starkly different shapes used in this study. It is therefore difficult for the neural network to interpolate accurately with limited training data. The study has however proved to a large extent, the feasibility of using one generalized neural network for predicting

profiles of defects with different shapes. This could prove to be significant milestone and a useful tool for the pipeline industry.

5.5 Future Work

Future work in this area should aim at a using a more comprehensive data set. This thesis presented work involving regular defect shapes and MFL signals obtained under controlled experimental conditions. Future efforts could be directed towards obtaining more data from real pipeline defects, which would also include irregular shaped defects.

Training the neural network with an extensive data set with signals from various different defect shapes would definitely lead to more accurate predictions.

Efforts could also be directed towards using other techniques to optimize center selection for the basis functions and the architecture of the neural network.

Research would also be required to quantitatively evaluate the accuracy of the predictions and associated confidence intervals, with the results.

REFERENCES

1. D. Bray and R. Stanley, "*Non-destructive evaluation - A tool in design, manufacturing and service*", CRC Press, Boca Raton, FL, 1997.

2. W. Lord, Class notes, EE448x, Spring semester, Iowa State University, 1994.

3. M. A. Abidi and R. C. Gonzalez, "*Data fusion in robotics and machine intelligence*", Academic Press, Boston, MA, 1992.

4. R. E. Beissner, G. A. Matzkin, C. M. Teller, "NDE applications of MFL methods - A state-of-the-art survey", Southwest Research Institute, San Antonio, TX, January 1980.

5. W. Lord and D. J. Oswald, "Leakage field methods of defect detection", International Journal of NDT, Vol. 4, pp. 249-274, 1972.

6. G. J. Posakony, "Assuring the integrity of natural gas transmission pipelines", Tropical Report, Gas Research Institute, GRI-91/0366, November 1992.

7. R. Davis, T. A. Bubenik, and A. Crouch, "The feasibility of magnetic flux leakage in-line inspection as a method to detect and characterize mechanical damage", Final Report, Gas Research Institute, GRI-95/0369, June 1996.

8. T. A. Bubenik, J. B. Nestleroth, R. J. Eiber, and B. F. Saffell, "Magnetic flux leakage (MFL) technology for natural gas pipeline inspection", Tropical Report, Gas Research Institute, November 1992.

9. G. Xie, "Defect characterization of gas pipelines using optimal radial basis function neural networks ", M. S. Thesis, Iowa State University, Ames, IA, 1996.

10. L. Udpa, S. Mandayam, S. Udpa, W. Lord, and Y. Sun, "Magnetic flux leakage inspection of gas pipelines : Neural networks for signal characterization, compensation and identification", Tropical Report, Gas Research Institute, February 1996.

11. V. E. Shcherbinin and N. N. Zatespin, "Calculation of magnetostatic field of surface defects, II. Experimental verification of the principal theoretical relationships", Defektoskopiya, Vol. 5, pp. 59-65, 1966.

12. W. Lord and J. H. Hwang, "Defect characterization from magnetic flux leakage fields", British Journal of NDT, pp. 14-18, January 1977.

13. R. Palanisamy and M. N. Curran, "Experimental evaluation of the accuracy of AC flux leakage and eddy current methods of sizing flaw depths in ferromagnetic seamless steel tubing", Materials Evaluation, Vol. 45, pp. 1398-1403, December 1987.

14. G. P. Singh and S. Udpa, "The role of digital signal processing in NDT", NDT International, Vol. 19, No. 3, pp. 125-132, June 1986.

15. L. Udpa and S. Udpa, "Application of signal processing and pattern recognition techniques to inverse problems in NDE", Int. J. of Applied Electromagnetics and Mechanics", pp. 99-117, August 1997.

16. Y. F. Cheu, "Automated crack detection with computer vision and pattern recognition of magnetic particle indications", Materials Evaluation, Vol. 42, pp. 1506-10+, November 1984.

17. S. Nair, S. Udpa, L. Udpa, "RBF networks for defect sizing", Proceedings of the Review of Quantitative Non Destructive Evaluation, San Diego, 1992.

18. M. Chao, "Neural networks for characterizing magnetic flux leakage signals", M. S. Thesis, Iowa State University, Ames, IA, 1995.

19. J. Aubin, *"Neural networks and qualitative physics - A viability approach"*, Cambridge University Press, New York, 1996.

20. W. S. McCulloch and W. Pitts, "A logical calculus of ideas immanent in nervous activity", Bulletin of Mathematical Biophysics, Vol. 5, pp. 115-133, 1943.

21. M. Minsky and S. Papert, "*Perceptrons : An introduction to computational geometry*", MIT Press, Cambridge, MA, 1969.

22. R. P. Lippman, "An introduction to computing with neural networks", IEEE ASSP magazine, pp. 4-22, April 1987.

23. D. B. Parker, "A comparison of algorithms for neuron-like cells", in J. S. Denker (Ed) Neural networks for computing, AIP conference proceedings, 151, Snowbird, Utah, 1986.

24. D. S. Broomhead and D. Lowe, "Multivariable functional interpolation and adaptive networks", Complex Systems, Vol. 2, pp. 321-355, 1988.

25. F. Luo and R. Unbehauen, "*Applied neural networks for signal processing*", Cambridge University Press, New York, 1997.

26. J. T. Tou and R. C. Gonzalez, "*Pattern recognition principles*", Addison-Wesley Publishing Company, Reading, MA, 1974

27. R. Fletcher and C. M. Reeves, "Function minimization by conjugate gradients", Computer Journal, Vol. 7, No. 2, pp. 149-154, 1964.

28. S. S. Rao, "*Optimization theory and applications*", Wiley Eastern, New Delhi, India, 1979.

29. E. Aarts and J. Korst, "*Simulated annealing and Boltzmann machines*", John Wiley and Sons, New York, 1989.

30. R. C. Luo and M. G. Kay, "Multisensor integration and fusion : issues and approaches", Proceedings of SPIE - Sensor Fusion, Vol. 931, pp. 42-9, Orlando, FL, April 1988.

31. R. C. Luo and M. G. Kay, "Multisensor integration and fusion in intelligent systems", IEEE Transactions on Systems, Man and Cybernetics, Vol. 19 (5), pp. 901-31, September/ October 1989.

32. R. C. Luo, M. Lin, and R. S. Scherp, "The issues and approaches of a robot multi-sensor integration", Proceedings of IEEE International Conference on Robotics and Automation, pp. 1941-46, Raleigh, March 1987.

33. T. Henderson, C. Hansen and B. Bhanu, "A framework for distributed sensing and control", Proceedings of 9th International Joint Conference on Artificial Intelligence, pp. 1106-9, Los Angeles, August 1985.

34. J. C. Pearson, J. Gelfand, W. Sullivan, R. Peterson, and C. Spence, "Neural network approach to sensory fusion", Proceedings of SPIE - Sensor Fusion, Vol. 931, pp. 103-8, Orlando, FL, April 1988.

35. M. Eggers and T. Khuon, "Neural network data fusion : concepts and application", IEEE Proceedings of International Joint Conference on Neural Networks, Vol. 2, pp. 7-16, San Diego, June 1990.

36. J. Rajapakse and R. Acharya, "Multisensor data fusion within hierarchical neural networks", IEEE Proceedings of International Joint Conference on Neural Networks, Vol. 2, pp. 17-22, San Diego, June 1990.

37. J. Yim, "Image fusion using multi-resolution decomposition and LMMSE filter", Ph.D. Dissertation, Iowa State University, Ames, IA, 1995.

38. P. C. Charlton, "Investigation into the suitability of a neural network classifier for use in an automated tube inspection system", British Journal of NDT, pp. 433-7, August 1993.

39. X. E. Gros, "*NDT Data Fusion*", John Wiley & Sons, New York, 1997.

40. S. Sharma, "*Applied multivariate techniques*", John Wiley & Sons, New York, 1996.

41. J. MacQueen, "Some methods for classification and analysis of multivariate observations", Proceedings of the fifth Berkeley symposium on mathematical statistics and probability, Vol. 1, pp. 281-97, 1967.

42. K. T. Hwang, S. Mandayam, S. Udpa, L. Udpa, and W. Lord, "A multiresolution approach for characterizing MFL signatures from gas pipeline inspections", presented at the Sixth IEEE Midwest Circuits Symposium, Ames, IA, August 1996.